Contents

List of Figures

List of Tables

Abstract

The El Niño-Southern Oscillation (ENSO) is a coupled ocean-atmosphere phenomenon which has its origins in the tropical Pacific ocean, yet it has a great impact on the Northern Hemisphere (NH) wintertime variability. The ENSO affects the circulation in the middle atmosphere through the propagation of the planetary Rossby waves and gravity waves. The latest version of the Whole Atmospheric Community Climate Model (WACCM) was used in our study to explore the ENSO effects. A filter was first applied to the observed Hadley Center Sea Ice and Sea Surface Temperature (HadISST) data set, which was then used in the WACCM model and provided us an model with only the ENSO-related variabilities.

Our aim was to study the climatology of the temperature, the zonal mean wind, the wave flux vectors and its divergence and the residual circulation. Then we wanted to see the how a warm ENSO event affected these parameters. We also looked into how these changes affected the trace gases transport. From our results we found significant wave-like anomalies observed in the stratosphere as well as in the mesosphere at middle latitudes with the most efficient wave propagation around 50^oN. We have shown that the wave activity is reflected in the pattern of the EP-flux. The results show that this wave propagation is strongly influenced by the zonal mean winds. This relationship is explained by the Charney-Drazin criteria: during the boreal winter, if stratospheric winds are westerly and their velocity is less than a critical value (which is strongly dependent the wave number and the latitude), then vertical wave propagation is possible.

The zonal mean temperature anomalies are observed in the middle atmosphere both in the tropical and polar regions of the NH. The modulation of the residual circulation are the reason for these temperature anomalies. During a warm ENSO event we observe an enhancement of the vertical wave propagation at middle latitudes and a divergence of the wave flux that indicates the weakening of the zonal mean zonal wind due to deposit of easterly momentum. Combined, this modulates our residual circulation. For the NH polar stratosphere, a weak ascent and a pattern of weakened BDC is observed, whereas a strong effect in the mesosphere with a strengthened pole-to-pole circulation is seen. Within this model run, consistency is observed between the residual circulation, EP-flux vectors and temperature. The residual circulation is closely linked to the trace gases transport and for methane and nitrous oxide there is a qualitative agreement, while the impact of the residual circulation on the ozone is less clear.

Acknowledgments

Firstly I am thankful to my supervisor Professor Frode Stordal for his continous help and enthusiasm during all stages of this thesis; from challenging me with the idea that has been the foundation of this project, making me aware of the differences in my data set compared to data sets used in previous works, to even checking my programming codes. Thanks for having your office door open at all hours and answering emails very late at night.

Another special thanks goes to Yvan Orsolini. Thanks for taking your time and giving me ideas on how to carry out my task. I would also extend my thanks to post-doc Sandeep Sukumaran for the model runs, without you this project would not have seen the light of day. Even though your current workplace is in Abu Dhabi, that would not stop you from replying to my emails in less than 30 minutes. I would like to extend my gratitude to Ole-Kristian Kvissel for lending me his code on studying the meridional circulation and of course thanks to Christine Smith-Johnsen, who spend several hours with me to understand how the code works and give me a crash course in a programming language I was not familiar with. Many thanks to study buddies and others at the Department of Meteorology and Oceanography (UiO) for creating a delightful atmosphere. What I have learned during my time here is certainly precious.

My biggest thanks goes to my dear Luc, whom supported and cheered on me the whole time. You are the best stress reliver and an incredibly patient and thoughtful person. Thanks for introducing me to the numerous board games and hopefully more to come. You are also extremely good at making excuses just to go travelling and discover new places with you. I am so grateful for having such a wonderful person in my life. I would like to specifically thank those who reviewed and proofread my thesis: Frode and Yvan, Christine and Luc.

CHAPTER 1

Introduction

The El Niño-Southern Oscillation (ENSO) is a coupled ocean-atmosphere phenomenon that causes inter-annual global climate variability and is one of the major concepts of climate dynamics. The main source of variability in the tropical troposphere is the ENSO, and the stratospheric circulation transmits the tropical ENSO signal into the mid-latitudes (Calvo et al. [2008]; Fernández et al. [2004]; García-Herrera et al. [2006]; Sassi et al. [2004]). Evidence from recent studies show that the extratropical upward wave propagation of ENSO intensifies during warm ENSO events in the Northern Hemisphere (NH) winter (Calvo et al. [2008]; García-Herrera et al. [2006]; Li et al. [2013]; Li and Lau [2012]). This affects the middle atmosphere by altering the meridional overturning circulation (Calvo et al. [2008]; García-Herrera et al. [2006]; Gerber et al. [2012]) and the polar vortex (Butler et al. [2014]; Li and Lau [2012]).

During a strong warm ENSO event, the meridional circulation in the tropical troposphere intensifies (Calvo et al. [2010]; García-Herrera et al. [2006]). Additionally, this upwards propagation and dissipation of planetary waves at middle and high latitudes leads to the acceleration of the stratospheric branch of the Brewer-Dobson circulation (BDC) (Butchart et al. [2006]; Calvo et al. [2010]; García-Herrera et al. [2006]). The region where the wave breaking occurs is often referred to as the "surf zone" (as will be discussed in Section 2.2.1). The breaking of waves deposits easterly momentum onto the background flow. These changes in the stratospheric mean meridional circulation also shows an effect on the stratospheric zonal mean temperature (Free and Seidel [2009]; Randel et al. [2009]), resulting in warmer polar stratosphere and a weaker polar vortex (Calvo et al. [2008]; García-Herrera et al. [2006]; Li and Lau [2012]).

Traditionally, the investigation of ENSO above the troposphere has been tricky due to a lack of global observations and the difficulty to decouple it from other variations such as the quasi biennial oscillation (Baldwin et al. [2001]). However, improvements of the general circulation models (GCMs) in recent years have demonstrated the propagation of the ENSO signal into the stratosphere (Calvo et al. [2008]; Free and Seidel [2009]; García-Herrera et al. [2006]; Li and Lau [2012]; Randel et al. [2009]). Today the effect of the ENSO signal in the stratosphere is well understood, however how great of an impact it has on the mesosphere is still debated (Li et al. [2013]; Sassi et al. [2004]).

Recent studies have revealed that the dynamics in the middle and upper atmosphere plays a

key role in both the tropospheric weather and climate. It is important to understand the role that atmospheric oscillations (in particular the gravity and planetary waves) have on this interaction. The origin of atmospheric mixing is the interaction of atmospheric oscillations with the mean-flow which is much of the large-scale atmospheric global circulations in the middle and upper atmosphere. The purpose of this thesis is to analyse results from a general circulation model, the Whole Atmosphere Community Climate Model (WACCM) on a monthly basis for the period 1955 - 2001 (more details in Section 3.1). The aim was to study the ENSO phenomenon and its impact on the middle atmosphere.

Two model runs from the latest WACCM version have been made available to me; the control-run (CTRL-run) using the observed global sea surface temperature (SST) anomalies from the Hadley Center Sea Ice and Sea Surface Temperature data set (HadISST) and another run (ENSO-run) only using the ENSO-related component of the same HadISST data set. Previous papers such as Calvo et al. [2008]; García-Herrera et al. [2006] based their analysis on a simulation that included all variabilities, like the CTRL-run. By doing so, the chosen strongest ENSO events became more evident, whereas the less strong ones became less apparent or could have been covered by other variabilities. The use of the ENSO-run is a novel approach to study ENSO impacts in the stratosphere, as previous studies did not have this second run available. The method of isolating the ENSO signal is described in Section 3.2 (see Compo and Sardeshmukh [2010]) for more details). The model results will illustrate the vertical wave propagation of the ENSO signal and the mechanisms by which this signal reaches the middle atmosphere.

In this thesis we will study the effect of the ENSO on the NH wintertime variabilities. We will start by looking at the climatology for the temperature, zonal mean zonal wind, Eliassen-Palm flux and its divergence and the mean meridional circulation. Then we will see how their patterns changes due to the impact of the ENSO by making composite maps. The vertical wave propagation in the stratosphere will be studied and its impact on the transport circulation will be investigated. Lastly we will try to see how these changes in the meridional circulation affects the trace gases. The theory behind this study is given in Chapter 2 with main focus on the middle atmosphere. The description of the basic datasets and analysis tools are described in Chapter 3. Chapter 4 presents the main results of the model run and the discussion part. Chapter 5 includes some suggestions for future work, and finally the conclusions and summary are presented in Chapter 6.

CHAPTER 2

Background Theory

This chapter is meant to give the reader a relevant background on the atmospheric circulation and transport processes relevant for understanding the impact of ENSO on the atmosphere. The ocean-atmosphere phenomenon is introduced in Section 2.1. Section 2.2 describes the vertical structure of the atmosphere with focus on the middle atmosphere and Section 2.3 focuses on the key features of the stratospheric dynamics and transport of the ozone and other trace gases, as well as other mechanisms that play a minor role. Section 2.4 reviews the most essential wave types important for transport in the stratosphere.

2.1 The tropical Pacific ocean-atmosphere system

The source of energy for motions in the ocean and atmosphere is ultimately solar radiation. Thus the ocean and atmosphere are in constant exchange of heat, water and momentum. Hence the oceanic conditions, in particular the sea surface temperatures (SSTs) are essential for atmospheric circulation and temperature conditions. The dominant mechanisms for heating the atmosphere are evaporation of water vapor from the surface, deep convection in cumulonimbus clouds and the consequently condensation and freezing. The convection into the atmosphere is strongly regulated by SST and at the same time modulates the ocean's surface momentum and heat fluxes. The interaction between the ocean and the atmosphere helps shaping the tropical climate and its variability.

2.1.1 The Pacific Walker circulation

The largest circulation cell oriented along the equator extending across the Pacific Ocean is known as the Walker circulation and is named after the meteorologist Sir Gilbert Walker [I], who

[I] Sir Gilbert Thomas Walker (1868-1958) was a British physicist and statistician. Before taking up a teaching position at Cambridge University, Walker studied mathematics in various applications including aerodynamics, electromagnetism and analysis of time-series data. Even though he had no experience in meteorology, he was recruited for a position in the Indian Meteorological Department. Here he identified the relation-

first described this phenomenon. This circulation is often referred to as the neutral state and is a zonal atmospheric circulation in the tropical Pacific, see Figure 2.1a for illustration. This is when trade winds transport the warm equatorial seawater to the west, which in turn accumulates at the eastern coasts of Indonesia. This leads to upwelling of cold water from the depths of the eastern Pacific at the coast of South America. As a consequence the warm water accumulated in the western Pacific leads to an ascent of the air masses and causes precipitation, this process is known as atmospheric convection and the cold water in the eastern Pacific leads to a descent of air masses (Holton and Hakim [2012, chapter 11]).

2.1.2 The El Niño - Southern Oscillation (ENSO)

As mentioned in Chapter 1, ENSO, is the most important mechanism describing the complex coupled ocean-atmospheric phenomenon in the tropical Pacific impacting the weather and climate patterns. The first two letters refer to El Niño[II], a recurrent pattern of positive sea-surface temperature anomalies in the equatorial Pacific and the second two letters refer to the linkage to the global pattern of sea-level pressure, which is known as the Southern Oscillation (Wallace and Hobbs [2006]). ENSO has three phases (see Figure 2.1):

Warm ENSO phase when SOI < 0

Neutral ENSO phase when SOI ≈ 0

Cold ENSO phase when SOI > 0

where SOI stands for Southern Oscillation Index. This index is based on the observed variations in sea level pressure between the Eastern Pacific and the Indian Ocean. El Niño, the warm phase of ENSO is characterized by an unusual warming in the eastern tropical Pacific. A weaker upwelling of cooler ocean waters from below also contributes to warmer SSTs. This generally occurs during the winter in the Northern Hemisphere (NH) with irregular intervals at 2-7 years. Leading to the large scale weakenings of the trade winds that usually blows westward from South America towards Asia. Other characteristics are reduced productivity of marine biosphere in the band of upwelling along the equator. The sea level rise in the equatorial eastern Pacific and lowering of sea level in the western Pacific, which is indicative of a weakening of the climatological-mean east-to-west gradient (Hartmann [1994, chapter 1], Wallace and Hobbs [2006, chapter 2]).

The opposite phase of El Niño is called La Niña[III], the cold phase of ENSO. During an La Niña event, the Walker circulation intensifies with greater convection over the western Pacific and stronger trade winds. La Niña events are characterized by increased rainfall over much of the northern and eastern Australia (Holton and Hakim [2012, chapter 11], Australian government - Bureau of Meteorology (`http://www.bom.gov.au/climate/enso/history/ln-2010-12/three-phases-of-ENSO.shtml`). El Niño and La Niña occur interannually and cause extreme floods and droughts in many parts of the world.

---

ship of the surface air pressure between the Indian and Pacific oceans and what is named after him. Source: `https://en.wikipedia.org/wiki/Gilbert_Walker`

[II]The term "El Niño" is Spanish and refers the Child Jesus, because the pool of warm water in the Pacific near South America is often at its warmest around Christmas. Source: `https://en.wikipedia.org/wiki/El_Nino`

[III]The term "La Niña" is Spanish and is litteraly translated to "the girl child". Source: `https://en.wikipedia.org/wiki/La_Nina`

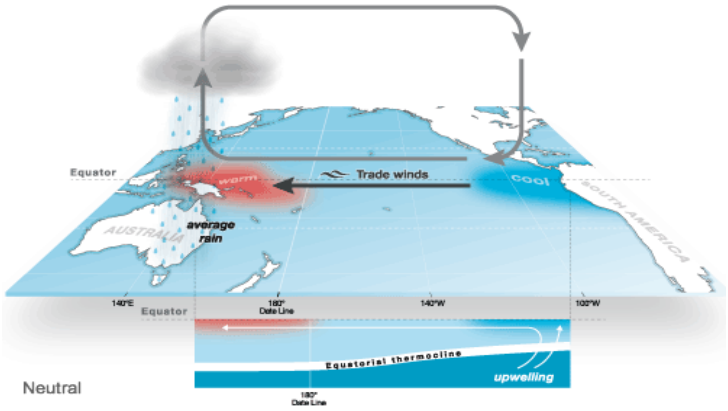

(a) Neutral ENSO event = normal Walker circulation

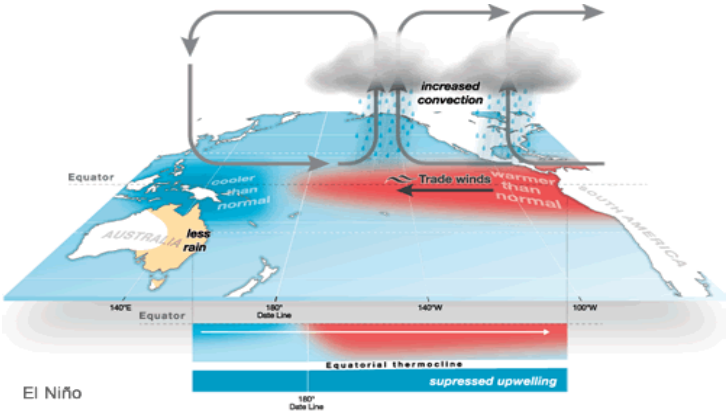

(b) Warm ENSO event = El Niño

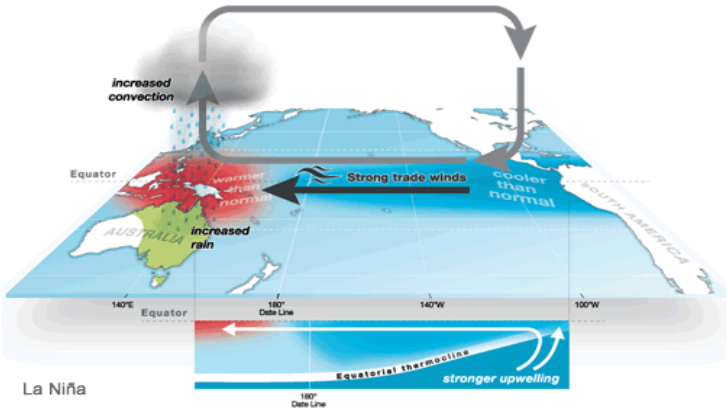

(c) Cold ENSO event = La Niña

Figure 2.1: (a) Neutral ENSO event: The air over Indonesia rises because of the low surface pressure and forms clouds. This eventually leads to heavy rainfalls over the western tropical Pacific throughout the year. The circulation of the air continues towards the region above the surface high pressure near Ecuador and is referred to as the Walker circulation. (b) Warm ENSO event: The winds can actually reverse and flow from west to east instead. This weakens the trade winds because the air pressure gradient between two pressure systems in the tropical Pacific decreases. (c) Cold ENSO event: The Walker circulation intensifies with stronger trade winds and greater convection over the Western Pacific. Figure courtesy by Australian Government, Bureau of Meteorology.

2.2 The general atmosphere

The atmosphere is a thin layer that surrounds the Earth and is divided into four layers based on the vertical temperature distribution, that is the troposphere, stratosphere, mesosphere and thermosphere. Two gases build up the main part of the Earth's atmosphere: nitrogen (N_2), which accounts 78 % of the atmosphere and oxygen (O_2), which accounts for 21 % and the remainder consists of various trace gases. Energy transfer between the Earth's surface and the atmosphere occurs through conduction, convection and radiation. Ocean currents play an important role in transferring heat poleward from the Equator, as well as contributing to the development of various types of weather phenomena (Wallace and Hobbs [2006]).

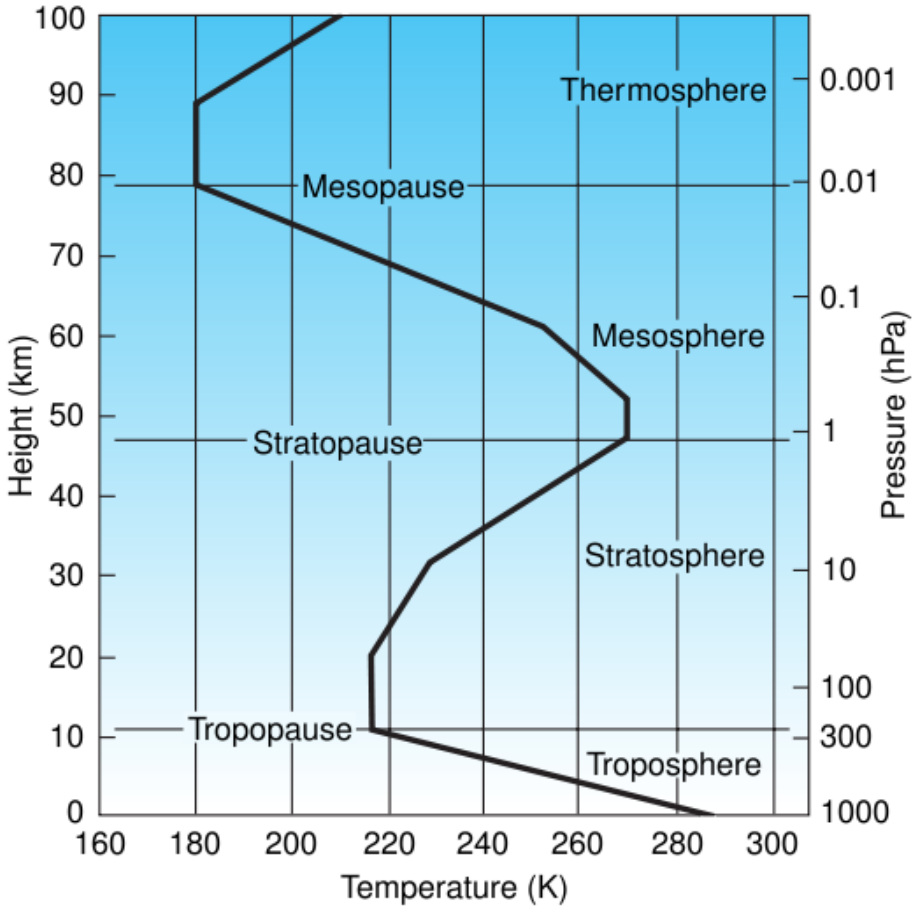

Figure 2.2: A typical midlatitude vertical temperature profile, as presented by the U.S. Standard Atmoshere (1976). Figure courtesy by Wallace and Hobbs [2006].

For a long time the atmosphere has been considered as a stratified medium with interactions between the troposphere and the upper layers. Figure 2.2 illustrates the structure of the atmosphere. The troposphere is the atmospheric layer (0 - 12 *km*) that lies above the ocean and is thereby directly affected by the state of the ocean. This layer is generally marked by decreasing temperature with height. Tropospheric air accounts for 80 % of the atmospheric mass and is relatively mixed. Above this layer is the stratosphere, where the temperature increases with height primarily from ozone absorption, extending from about 12 *km* and up to 50 *km* in altitude. Unlike in the troposphere, stratospheric air is quite thin and gets thinner with increasing

altitude. Stratospheric air is also very stable, thus the vertical motion in the stratosphere is slow.

Above the ozone layer lies the mesosphere with decreasing temperature with height. The mesosphere has a lapse rate similar to that in the troposphere, extending from the stratopause to the mesopause at about 80 - 90 *km*. The outermost layer is called the thermosphere where temperature increases with height due to absorption of solar radiation (Hartmann [1994, chapter 1],Wallace and Hobbs [2006, chapter 2]).

Generally the middle atmosphere is regarded as the region above the tropopasuse (about 10 - 16 *km* depending on the latitude) up to about 100 *km*. The stratosphere and mesosphere layers are considered as part of the main bulk as depicted in Figure 2.2. As mentioned earlier in Section 2.2 the troposphere accounts for about 80 % of the atmosphere's total mass. There is no doubt that processeses occurring within the troposphere are the main responsible for weather interferences and climate variability. However the middle atmosphere cannot be disregarded.

The linkage between the troposphere and the middle atmosphere are through the radiative and dynamical processes that are importanct in aspects of global forecast and climate models. As briefly mentioned above it has become increasingly recognised that resolving the stratosphere and modelling its variability is necessary to correctly simulate tropospheric weather and climate (Marsh et al. [2013]). Furthermore, they are also connected through the exchange of trace substances that are essential in the photochemistry of the ozone layer (Free and Seidel [2009]; García-Herrera et al. [2006]; Li and Lau [2012]; Manzini [2009]; Randel et al. [2009], Holton and Hakim [2012, chapter 12]).

The middle atmosphere has little thermal inertia thus the flow tends to be far more zonally symmetric than the tropospheric flow, making the zonal average more physically meaningful. In the sense of time-averaging, air moves predominantly in the east-west direction and dynamical and chemical fields are mostly uniform along constant-latitude circles. Zonal averaging indicates how the large-scale vertical and meridional circulation systems are generated Brasseur et al. [1999, chapter 2].

2.2.1 The stratosphere's structure

The stratosphere can be characterized by four distinct regions summed up in bullet points $(\mathbf{1}) - (\mathbf{4})$ below. Figure 2.3 depicts the winter/summer conditions in the Northern Hemisphere (NH)/Summer Hemisphere (SH), as well the driving sources of the meridional circulation in the atmosphere and its distinctive $((\mathbf{1}) - (\mathbf{4}))$ regions.

(1) the tropics, which stretch from about 20 ^{o}N to 20^{o}S;

(2) the middle latitudes or "surf zone";

(3) the polar vortex and

(4) the lowermost stratosphere

The photochemical source region for ozone lies in the tropics (region stretching from 20^oN - 20^oS) as sufficient energetic ultraviolet radiation from the Sun hits this area to create ozone. This ozone is then transported out of this region and poleward by a broad circulation pattern described in Section 2.3.1. The surf zone or the middle latitudes of the stratosphere is the region where turbulent overturning and rapid meridional mixing happens. This occurs when

atmospheric waves grow to large amplitudes and break. The process of wave breaking causes wave dissipation or damping (more details in Section 2.3.5).

The mixing of air masses, each with different amounts of ozone gives the surf zone a turbulently mixed appearance, which is due to the equator-to-pole circulation pattern. Tropical air contains less ozone than polar air and as a result of weather patterns in the middle latitudes, tropical and polar air are blended together (Plumb [2002], Cordero et al. [2013, chapter 6]).

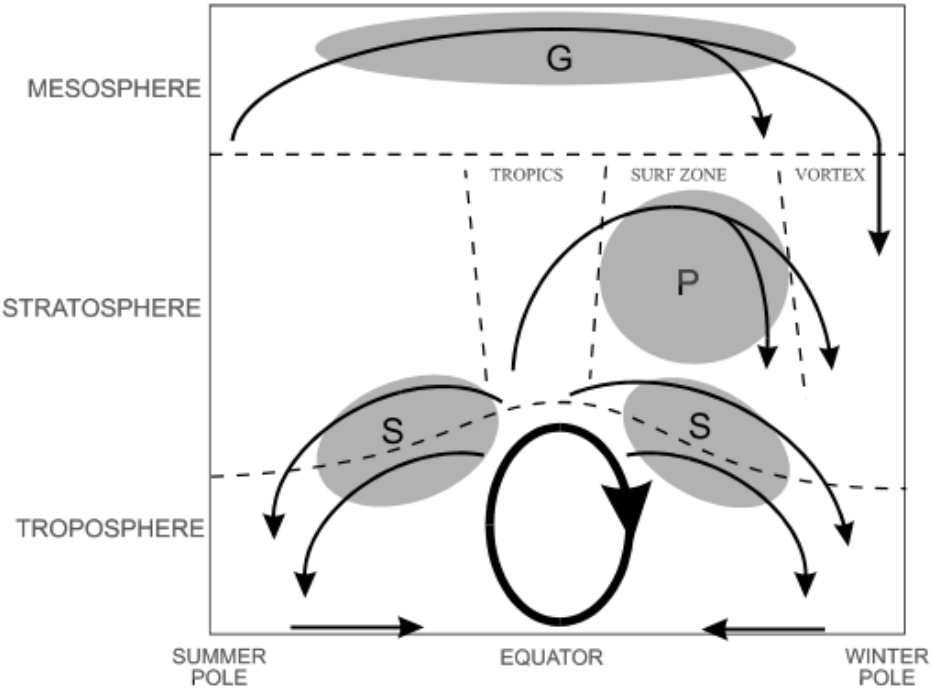

Figure 2.3: Schematic of the residual mean meridional circulation in the atmosphere. The heavy ellipse denotes the thermally-driven Hadley circulation of the troposphere. The shaded regions (labelled “S”, “P”, and “G”) denote regions of breaking waves (synoptic- and planetary-scale waves, and gravity waves, respectively), responsible for driving branches of the stratospheric and mesospheric circulation. Thin dashed line in the horizontal denotes the tropopause, while the vertical dashed lines denote the distinctive regions of the atmosphere. Figure courtesy by Plumb [2002].

During the Northern Hemisphere winter, the lower middle stratosphere is characterized by strong and almost zonally and symmetric westerly flows in subpolar latitudes, whereas weaker easterly winds prevail in summer. The wintertime stratospheric winds are at the same time on the level of the Jet Stream winds. Cooler temperatures in the stratosphere over the Arctic is connected to the positive phase of the Artic Oscillation and indicates stronger polar winds. This westerly flow pattern is known as the stratospheric polar vortex. The considerable reduction of the incoming solar radiation causes cooling of the northern polar region and thermally drives the poalr vortex.

In general the vortex is formed in early winter, wheras it normally decays in late winter to early spring when circulation resets back to the summer situation. An example would be a

sudden stratospheric warming. This happens when the normal winter-time polar vortex breaks down due to the propagation and breaking of planetary waves from the troposphere, see Figure 2.6 for illustration (Calvo et al. [2008]; Shepherd [2007], Holton and Hakim [2012, chapter 12]). In the equatorial middle atmosphere the zonal mean flow is greatly affected by vertically propagating waves. The interaction between these waves and the mean flow produces a long period oscillation called the quasi-biennial oscillation (QBO).

Lastly a special region of the stratosphere is named the lowermost stratosphere. This region contains a mix of both tropospheric and stratospheric air masses and each air mass has its own chemical composition (Newman and Todara [1996, chapter 2], Plumb [2002]).

2.3 Transport in the middle atmosphere

This section reviews the dynamic interactions of the middle atmosphere; from covering the theory of Brewer-Dobson circulation to how wave activity influences the stratospheric circulation during wintertime, as well as the distribution of tracer constituents and other circulations that also affect the ozone transport.

2.3.1 Theory of Brewer-Dobson circulation (BDC)

The meridional circulation of the stratosphere is often referred to as the Brewer-Dobson circulation (BDC), describing the equator to pole transport of trace gases in the stratosphere. This circulation is named after Brewer (1949)[IV] and Dobson (1956)[V] from observations of stratospheric water vapor and ozone (Brasseur et al. [1999]; Cordero et al. [2013]; Newman and Todara [1996]; Plumb [2002]). This circulation model explains why the tropical air is lower in ozone concentration than polar air, even though the source itself is situated in the tropics (Plumb [2002]; Wallace and Hobbs [2006]).

The BDC consists of a two-cell structure in the lower stratosphere, with upwelling in the tropics from the troposphere into the stratosphere and subsidence in middle and high latitudes and a single cell from the tropics into the winter hemisphere at higher altitudes. However, it should be noted that the middle latitude descending air is transported back into the troposphere, while the high or polar latitude descending air is transported into the polar lower stratosphere, where it accumulates, see Figure 2.4 for schematic.

The mechanism behind the BDC is both complex and fascinating. From statements so far one would assume the reason for the existence of BDC to be solar heating in the tropics and cooling in the polar region, causing a large equator-to-pole overturning of air as warm, light (tropical) air rises and cold, dense (polar) air sinks. After all this heating and cooling does indeed occur, and this meridional overturning is the so-called Hadley circulation (see Figure 2.4). Yet, this is not the actual reason for the existence of the BDC. Instead the BDC results from wave activity in the extratropical stratosphere. For more thorough discussion of waves, see Section 2.4. In the absence of any stratospheric waves and thereby the BDC, the polar

[IV] Alan West Brewer (1915 - 2007) was a Canadian-English physicist and climatologist and began working for the Met Office in 1937. While researching for the Royal Air Force during the World War II, he made the discovery of the stratosphere being much drier than expected.

[V] Gordon Miller Bourne Dobson (1889 - 1976) was a British scientist who devoted most of his life to the observation and study of ozone. His work were to be of great importance in understanding the structure and circulation of the stratosphere.

region in the middle of the winter would be far colder that it actually is (Brasseur et al. [1999]; Cordero et al. [2013]; Newman and Todara [1996]).

As emphasized the BDC transfers mass and trace chemicals upward across the tropopause in the tropics and downward in the extratropics. The fact that this schematic is correct will also be quantified in Section 2.3.4. Through this section we have learned the about the general pattern of the BDC, which features rising motions around the equator, poleward transport and sinking motion in the highter latitudes. However, there are major hemispheric differences regarding strength and behaviour of the BDC cell. Later in Section 4.1 we will examine the large-scale features of the zonal mean distributions of temperature, zonal wind, ozone and traces gases in the stratosphere (Cordero et al. [2013]).

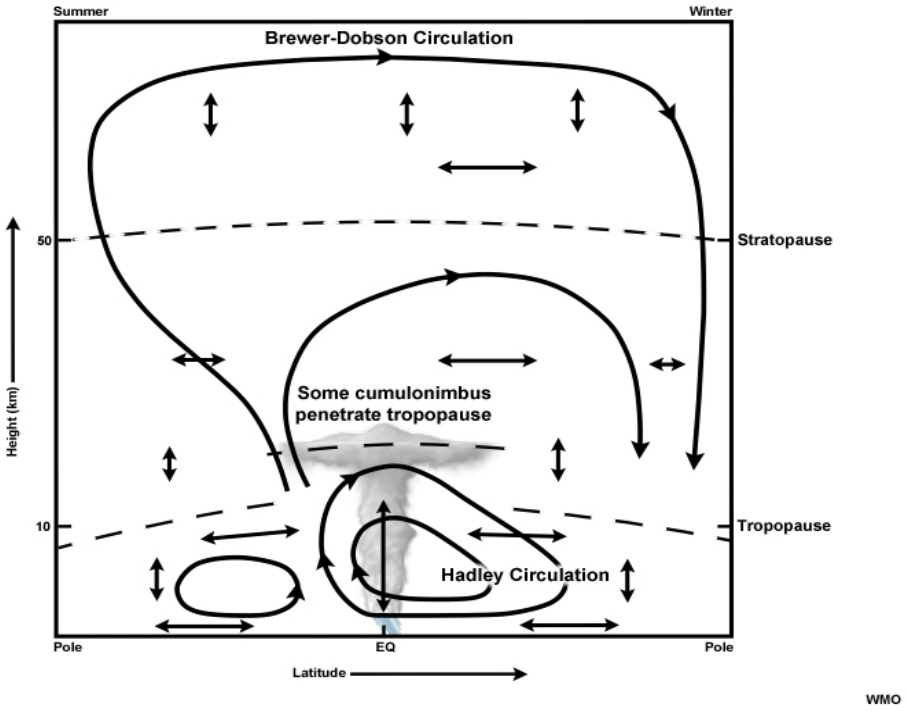

Figure 2.4: Schematic diagram of the Brewer-Dobson stratospheric circulation. Note that much of the stratospheric air enters through the tropical tropopause. Figure courtesy by WMO - World Meteorological Organization, 1985.

2.3.2 Transformed Eulerian mean (TEM)

To study the sources responsible generating the zonal mean zonal wind variability, the role of different forcing mechanisms need to be examined. Since the BDC describes a Lagrangian-mean transport it can not be diagnosed directly from the Eulerian velocity fields in the models(Holton and Hakim [2012]). The equations for the (TEM) residual circulation was introduced by Andrews and McIntyre [1976, 1978] and is used to approximate the BDC in dynamical models. The mean meridional and vertical velocities are defined as:

$$\overline{v}* = \overline{v} - \frac{1}{\rho_0}\frac{\partial}{\partial z}\Big(\frac{\rho_0\overline{v'\theta'}}{\overline{\theta}_z}\Big) \tag{2.1}$$

$$\overline{w}* = \overline{w} + \frac{\partial}{\partial y}\Big(\frac{\overline{v'\theta'}\cos\phi}{\overline{\theta}_z}\Big) \tag{2.2}$$

Equation 2.1 and 2.2 are the so-called residual Eulerian mean or TEM velocities. And are related to continuity equation by:

$$\frac{1}{\cos\phi}\frac{\partial\cos\phi\overline{v}*}{\partial y} + \frac{1}{\rho_0}\frac{\partial\rho_0\overline{w}*}{\partial z} = 0 \tag{2.3}$$

The zonal mean momentum in the TEM system is:

$$\frac{\partial\overline{u}}{\partial t} + \overline{v}*(\frac{1}{\cos\phi}\frac{\partial\overline{u}\cos\phi}{\partial y} - f) + \overline{w}*\frac{\partial\overline{u}}{\partial z} = \frac{1}{\rho_0\cos\phi}\nabla\cdot\mathcal{F} \tag{2.4}$$

where $\mathcal{F}$ is the Eliassen-Palm flux, a vector in latitude/height plane defined as $\mathcal{F} = (\mathcal{F}_\mathbf{y}, \mathcal{F}_\mathbf{z})$ with

$$\mathcal{F}_\mathbf{y} = \rho_0\cos\phi\Big(\overline{u}_z\frac{\overline{v'\theta'}}{\overline{\theta}_z} - \overline{u'v'}\Big) \tag{2.5}$$

$$\mathcal{F}_\mathbf{z} = \rho_0\cos\phi\Big[\Big(f - \frac{1}{\cos\phi}\frac{\partial\overline{u}\cos\phi}{\partial y}\Big)\frac{\overline{v'\theta'}}{\overline{\theta}_z} - \overline{u'w'}\Big] \tag{2.6}$$

See Chapter 2 in Brasseur et al. [1999] for more details about the abovementioned equations. In short the most important features of the TEM system is that it quantifies the zonal momentum forcing (Equation 2.4), $\mathcal{F}$ is proportional to the "wave activity" flux and show sources and sinks of waves, while Equation 2.5-2.6 indicates the direction of wave propagation. The Eliassen-Palm flux will be discused in more details in Section 2.3.3.

2.3.3 Eliassen-Palm flux (EP flux)

The Eliassen-Palm flux (EP flux) is an idealized primitive equation of the atmosphere. The EP flux vector measures the total effect of the eddies on the zonal mean flow. Eddy heat and momentum fluxes are dependent on each other. As previously mentioned, planetary waves have a strong influence on the zonal mean wind based on the wave-mean flow interaction theorem (Andrews and McIntyre [1976]; Charney and Drazin [1961]). Often this wave stress is directly responsible for causing atmospheric instabilities and thus creating atmospheric turbulence. Large regions of the atmosphere becomes homogenized through wave perturbation.

When the EP-flux vector points in the meridional direction ($\mathcal{F}_\mathbf{y}$), the meridional flux of the zonal momentum[VI] caused by atmospheric waves dominates. The EP flux vector can be positive as well as negative in y-direction, meaning that there could be transport of positive momentum towards the poles as well as towards the equator.

When the EP-flux vector points upward ($\mathcal{F}_\mathbf{z}$), the meridional heat flux dominates. However, $\mathcal{F}_\mathbf{z}$ is somewhat harder to understand. This vector indicates the division between two terms; the nominator refers to the meridional heat flux due to waves. Meaning winds bringing warmer air along towards the pole, gives a positive heat flux towards the pole, and can be interpreted as a flux of heat caused by waves. The term in the denominator is the change of potential temperature with pressure level or the change of potential temperature with height. Knowing the fact that temperature decreases poleward (in the stratosphere), means that there is always a (positive) heat flux from the equator the pole (heat being carried from the equator to the pole). Only keep in mind that the magnitude of this meridional heat flux is influenced by the presence/absence of wave 1 or wave 2. The potential temperature with height is also positive, meaning that the z-vector of $\mathcal{F}$ is always positive as seen in Figure 4.2b.

The divergence of the EP-flux acts as a zonal mean force applied to the zonal mean flow. Equation 2.4 implies that the eddies can produce an acceleration of the zonal mean flow, $\overline{u}_t$, only when the divergence of the EP-flux is non-zero (Brasseur et al. [1999]). Negative values of the divergence of EP-flux lead to decelerated westerlies, whereas positive values of the divergence of EP-flux leads to accelerated Westerlies.

2.3.4 Chemistry transport

Changes in the stratospheric circulation and temperatures such as on interannual basis and long-term are of interest for several reasons, in particular in understanding the 'recovery' of the ozone layer (Hardiman et al. [2007] and references therein). The residual circulation shapes the thermal and chemical structure, strongly influences the transport and composition in the stratosphere. In the winter hemisphere the BDC controls how cold the Arctic temperature becomes every winter as well as the increase of ozone through the poleward transport and downwelling.

Air is transported and distributes chemical properties from one region of the atmosphere to another. Through this transport process different chemical species with different local sources interact (Brasseur et al. [1999]; Wallace and Hobbs [2006]). As an example the distribution of N_2O is shown in Figure 2.5. Nitrous oxide (N_2O) is a 'tropospheric source gas' and its behaviour reflects the BDC and eddy mixing. A strong vertical stratification is notable due to photochemical destruction (radiation) in the stratosphere. In the equatorial region, upward bulging mixing ratio isopleths are evidence of upward mass flow, whereas in high latitudes downward sloping isopleths are evidence of subsidence in the polar regions. Near the surface N_2O is produced and is uniformly mixed in the troposphere and acts as a source of reactive nitrogen (NO, NO_2) in the upper stratosphere and is important for stratospheric ozone (O_3).

Methane (CH_4) is another tropospheric source gas that oxidizes to H_2O in the upper stratosphere. During the boreal winter, the downward circulation is stronger between 60^oN - 90^oN, whereas (not shown) the downward circulationd during boreal summer is noticeably weaker.

[VI]The momentum is the tendency of a particle's movement. Thus, a particle with more momentum moves generally faster. The same kind of concept applies for large scale system such as pressure system. When a gradient in pressure becomes larger toward the north,the transport of momentum increases.

Observation shows that methane has a higher concentration in the Arctic winter than the Antarctic winter. As discussed in Section 2.4, the downward circulation is greater in the boreal winter than in the aureal winter, thus greater amounts of CH_4 in the Arctic than in the Antarctic. This is because of stronger wave activity in the NH leads to more meridional mixing of air from lower latitudes into Arctic than into the Antarctic. Air that ascends into the Arctic lower stratosphere has been mixed with higher concentration of methane from the northern middle latitudes stratosphere. Whereas weaker wave activity in the SH causes less meridional mixing as can be seen in Figure 4.5b. Air that descends into the Antarctic lower stratosphere is more or less unmixed lower methane mesospheric air carried down by the descending branch of the BDC. Thus low wintertime CH_4 concentration in the Antarctic than in the Arctic. Understanding the transport in the middle atmosphere provides insight of its key features such as the stratospheric surf zone, mixing barriers and more (Brasseur et al. [1999]; Shepherd [2007]). The winter stratosphere is characterized by very low temperatures due to the absence of solar heating and a strong eastward flow around the pole (the "polar vortex") as illustrated in Figure 2.6. This condition permits propagation of the planetary waves into the winter stratosphere as described in Section 2.2.1.

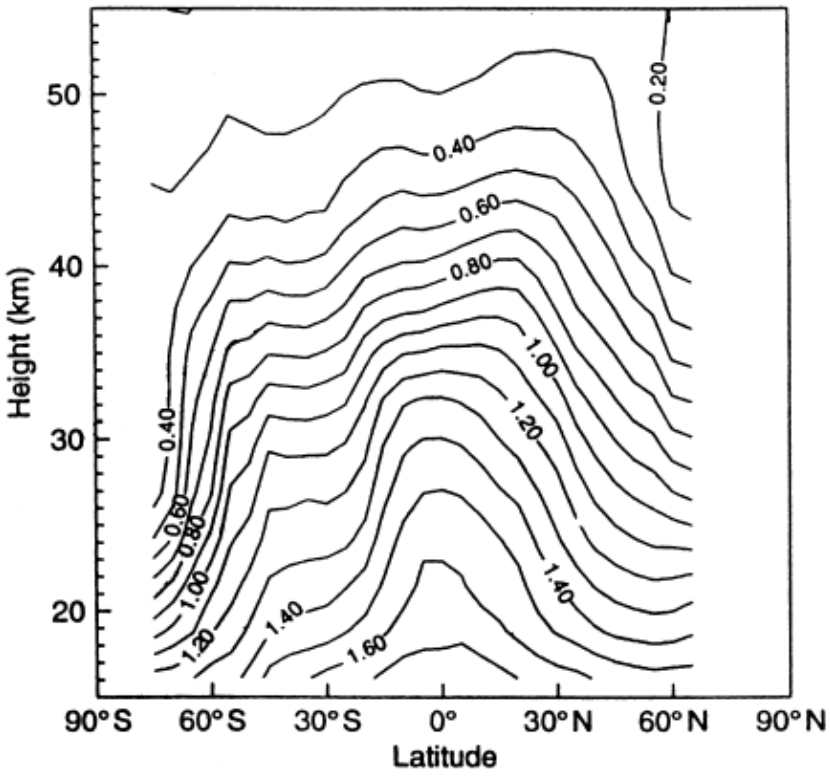

Figure 2.5: October zonal mean cross section CH_4 ($ppmv$) from observations by the Halogen Occultation Experiment (HALOE) on the Upper Atmosphere Research Satelite (UARS). Figure courtesy Holton and Hakim [2012] and references therein.

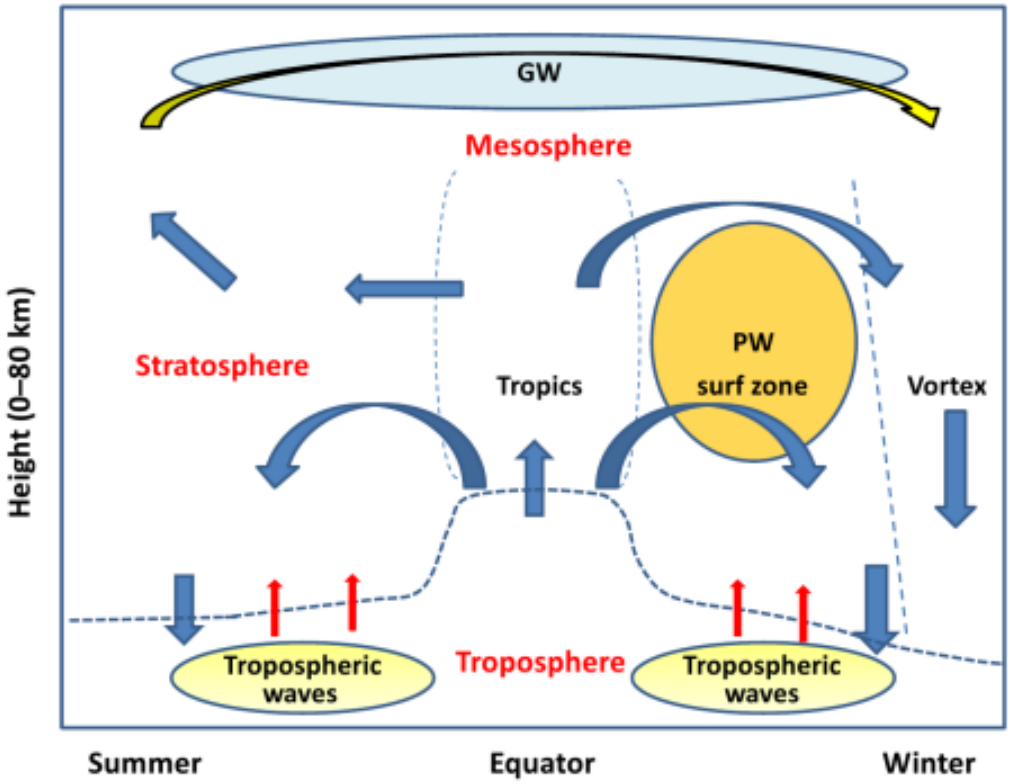

Figure 2.6: Dynamical interactions of the troposphere-stratosphere-mesosphere. Transport by the Brewer-Dobson circulation (BDC) is shown by the thick blue arrows. In the lower part of the stratosphere, the BDC transports air from the tropics into both hemispheres and then downward through the tropopause. As depicted the BDC has a strong poleward, downward circulation in the winter hemisphere where breaking of the planetary waves occurs. For the summer hemisphere, the upper circulation is poleward and upward. The yellow arrow shows the pole-to-pole transport in the mesosphere. Here the dominating energy source are the gravity waves. The red arrows indicate the source of tropospheric wave energy propagating into the stratosphere throughout the year. The vertical dashed thin blue lines indicate regions of restricted two-way transport ("mixing barriers"). The tropopause is denoted by the dashed thick blue line. Figure courtesy by Encyclopedia of Atmospheric Sciences, Volumer 1-6.

2.3.5 Mixing and distribution of long-lived tracers

The vertical dashed thin blue lines in Figure 2.6 depicts the mixing barriers. The mixing indicate the restricted transport between the barriers induced by wave motion. Wave motion in the stratosphere is close to being adiabatic, meaning that mixing is mainly quasi-horizontal (along isentropic surfaces). This quasi-horizontal mixing causes the flattening of the latitudinal tracer gradients as described in the above example. N_2O in Figure 2.5 exhibits the characteric shape for distribution of long-lived tracers, bulging upwards in the tropics and downwards in the extratropics because of the BDC but smoothened out by the mixing. This feature is highly recurring for all long-lived species as transport affects them in the same manner (Shepherd [2007]).

Also observed in Figure 2.5 is that horizontal mixing in the stratosphere is fairly spatially inhomogeneous. Between the subtropics and at the edge of the polar vortex around 60^oS, strong latitudinal gradients can be detected. These latitudinal gradients of long-lived tracers suggest an inhibiting behaviour towards the horizontal mixing, and is commonly referred to as a "mixing barrier" (Brasseur et al. [1999]; Shepherd [2007]). The mixing barrier is followed by the region called the stratospheric surf zone (see Figure 2.6). The surf zone arises from breaking of planetary waves (when the wave amplitude becomes to large) and acts to homogenize long-lived tracers within the surf zone. This process causes air parcels to undergo strong, irreversible, meridional mixing. The strength of the mixing is directly related to how strong the waves are (Brasseur et al. [1999]; Cordero et al. [2013]; Newman and Todara [1996]). This means that during the boreal midwinter greater mixing occurs than during the aural winter.

2.3.6 Other meridional circulation patterns

Until now the stratosphere has been our main focus but through Figure 2.3, 2.4, 2.6 we get clues that there are other circulation patterns outside the stratosphere that also affects the distribution of ozone. First and foremost we will now focus on the atmospheric circulation patterns in the meridional direction, that is the north-south direction. These circulations are to be localized both in the troposphere and the mesosphere.

BDC is by far the most important circulation for understanding stratospheric ozone but other circulations still remain important. The Hadley circulation (Figure 2.4) is a tropospheric circulation that rises in the tropical troposphere and descends over the extratropical region. In the tropical troposphere warm air rises along the Inter-Tropical Convergenze Zone (ITCZ), creating penetrating towers of cumulonimbus driven by convergence into the atmosphere. By doing so, it brings material from the surface and into the tropical upper troposphere and carry ot slowly into the stratosphere. This cell ends with air sinking back down in the cooler subtropical regions, leading to subsidence and bands of semipermanent high pressure. This cell pattern is the Hadley circulation (Cordero et al. [2013, chapter 6]).

A single circulation cell is dominating the upper stratosphere through the mesosphere during solstices (Figure 2.4). The circulation starts with rising motion in the summer hemisphere and sinking motion in the winter hemisphere. This corresponds to a summer-to-winter hemisphere meridional drift as required by mass continuity (Figure 4.4). This results in a much colder summer polar mesosphere than its radiative equilibrium in contrast to a much warmer winter polar mesosphere (Figure 4.1a). Small scale gravity waves are driving this circulation cell. These waves emerges for every seasons at all latitudes in the mesosphere (Hartmann [1994], Cordero et al. [2013]).

2.4 Vertically propagating waves

Waves can transmit heat and momentum far away from its origin and therefore be of great influence globally. Similar to ocean waves, these waves can either displace tracer constituents for a short time or permanently (Cordero et al. [2013, chapter 6]). The waves are primarily generated in the troposphere and from there they propagate upward. A variety of processes (Section 2.3) are induced by tropospheric waves (Figure 2.6). This section will review some of the most important waves relevant for transport in the stratosphere: the planetary Rossby waves

and gravity waves.

2.4.1 Planetary Rossby waves

In the general atmospheric circulation, the propagation of planetary waves is controlled by the atmospheric mean flow. This may lead to great deviations of the background zonal mean flow through deposition of zonal momentum by planetary waves. Their importance is strongest in the middle- and high latitudes. The first study on vertical planetary wave propagation was done by Charney[VII] and Drazin[VIII] (1961) and was based on linear wave theory (Andrews and McIntyre [1976]; Charney and Drazin [1961]. Section 2.3.1 described the generation of Rossby waves in troposphere (Figure 2.3 and 2.4), which propagates vertically into the stratosphere and grows in size as they go upward (air is less dense in the stratosphere). They propagate vertically along the axis of the jet core (Figure 4.1b illustrates the zonal mean zonal winds) and bends eventually towards the tropics (Figure 4.2 and 4.10). This wave propagation causes deceleration of the polar (night) jet and will be discussed more throughout Chapter 4.

The stratosphere is predominated by the these vertically propagating quasi-stationary planetary Rossby waves in the NH winter (named after Carl Gustav Rossby[IX], an early atmospheric research scientist). Principally responsible for driving the BDC are the Rossby waves (Figure 2.3). Planetary Rossby waves exists due to the equator to pole gradient of potential vorticity and arises from flow over topography and by temperature contrasts between land or ocean. These waves can propagate vertically provided that the mean zonal wind is westerly and less than a critical value that is strongly dependent on the wavelength of the waves and the latitude according to the Charney-Drazin criteria (CD criteria). This criteria implies that only ultra-long wave are able to propagate from the troposphere to the stratosphere in the middle- and high latitudes (Charney and Drazin [1961]).

These waves are dynamically important in the stratosphere because they provide a great part of the total eddy momentum and heat fluxes and explain the large deviations between the observed wintertime temperature in the northern polar stratosphere and the radiative equilibrium temperatures. When this wave propagation reaches the stratosphere it can alter the stratospheric circulation significantly where they break and get absorbed (Figure 2.3), which is also referred to as wave dissipation and growth and occurs as a result of meridional exchange or transport of air in the stratosphere. During the northern winter at high latitudes, periods of rapid growth of planetary waves are quite common. This rapid wave growth can cause sudden and extreme changes in the temperature and circulation structure.

Planetary wave activity also causes hemispheric differences. Later on we will learn that the BDC cells in the SH and NH are significantly different. These differences arises from the hemispheric differences in planetary wave forcing leaving the troposphere. The NH features large-scale tropography such as the Rockies and the Himalayas, while the SH has significantly

[VII] Jule Gregory Charney (1917 - 1981) was an American Meteorologist who contributed to the development of numerical weather prediction. Charney developed a set of equations for to understand baroclinic instability and is vital for the understanding mid-latitude cyclones. He is considered as the father of modern dynamical meteorology.

[VIII] Philip Gerald Drazin (1934 -2002) was a British mathematician and was a leading international expert in fluid dynamics. He pioneered in the work on hydrodynamic instability and the transition to turbulence.

[IX] Carl-Gustaf Arvid Rossby (1898 - 1957) was a Swedish born American meteorologist. He was the first one to explain the large-scale motions of the atmosphere in terms of fluid mechanics. He discovered and characterzied both the jet stream and the long waves in westerlies, the latter were named Rossby waves.

less land and consists of substantially only ocean (Cordero et al. [2013]; Hartmann [1994]). For instance the weak winter wave activity in the SH indicates a more isolated Antarctic polar vortex than its Arctic counterpart. This results in a strong vortex with extremely strong winds and low temperatures. These differences in wave forcing have a great influence on transport and lead to the observed hemispheric differences in distribution of ozone and other stratospheric trace components (Section 2.3.4). The striking topography- and land-ocean contrasts between the two hemispheres is why we in the boreal winter stratosphere observe more frequent and intense planetary wave activity than in the austral winter stratosphere. This pronounced wave activity in the boreal winter causes a stronger BDC than during the aural winter

2.4.2 Gravity waves

Gravity waves or buoyancy waves can arise from either the stability (changes of potential temperature with height or the buoyancy of air in a stably stratified atmosphere). In recent years research activity have focused on gravity waves in the atmosphere. Gravity waves have a number of effects and major contributions on atmospheric circulation, structure and variability. Aside from their occasionally strong lower-atmospheric effects, the major impacts occur in the middle atmosphere, between 10 and 100 *km* (i.e from the upper troposphere to the thermosphere) (Fritts and Alexander [2003]).

These waves involve vertical displacement of air parcels along slanted paths and are to be found everywhere in the atmosphere. Their propagation is both in the vertical and horizontal direction, transporting momentum from their source to their sink. While Rossby waves are primarily responsible for the BDC, gravity waves governs the entire circulation of the stratosphere and mesosphere. It is therefore important to quantify the influence of gravity waves in terms of climate change scenarios. They can have a major contribution to the momentum- and chemical compounds budgets. Multiple studies have shown that General Circulation Models (GCMs) produce a more correct view of the wind distribution when parameterized gravity wave processes have been included (Brasseur et al. [1999] and references therein).

The winds in the stratosphere filter the gravity waves either by reflection or absorption at the critical layer. Under normal winter conditions in the NH, the mesosphere is dominated by westward propagating gravity waves. Like for Rossy waves, wave breaking can also occur for very small gravity waves. Gravity waves can grow rapidly to generate convective instability, overturning and rapid vertical mixing of air from different origins - therefore the breaking of gravity waves are important to avoid this from happenening. As briefly mentioned in Section 2.3.6, gravity waves also affect the mean meridional circulation by decelerating the mean flow in the upper stratosphere and mesosphere. Momentum is tranported by these wave vertically, where the momentum is important to the large-scale momentum balance of the stratosphere and mesosphere.

CHAPTER 3

Data and Methods

The model runs for this thesis were simulated for the period 1955-2001 from the Whole Atmosphere Community Climate Model (WACCM), (Marsh et al. [2013]) and produced by Sandeep Sukumaran. Sandeep Sukumaran was a former post-doc of Professor Frode Stordal at the Department of Geosciences, University of Oslo (UiO). The observed Hadley Center Sea Ice and Sea Surface Temperature (HadISST) (Rayner et al. [2003]) data set was used in the latest WACCM model version and gave us one output referred to as the control-run (CTRL-run). In order to estimate the ENSO-related contribution to stratospheric variability, a filter (Compo and Sardeshmukh [2010]) was applied to the same HadISST data set to give us a secound output that only included the ENSO-related component. This data set is referred to as the ENSO-related-run (ENSO-run) and our study is based on this simulation. Figure 3.1 is a simple overview on how Sandeep Sumuaran produced our datasets.

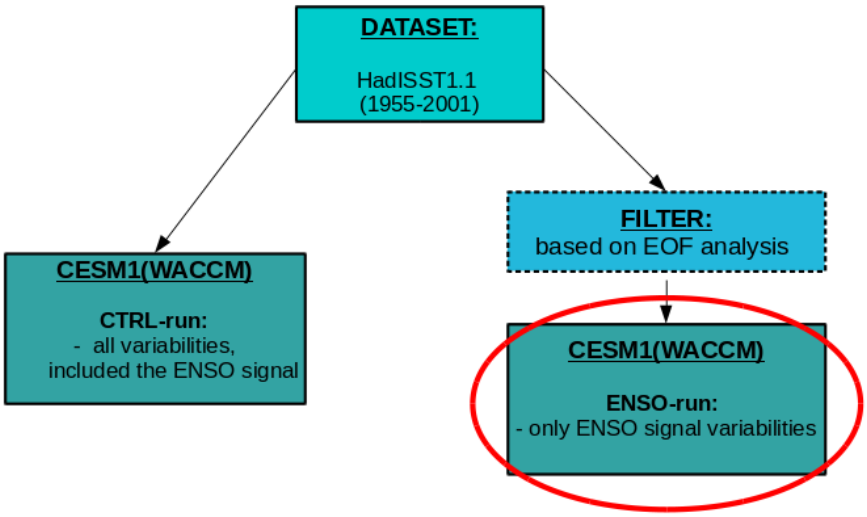

Figure 3.1: Schematic over our analysis tools and datasets. Thick red line marks the dataset (ENSO-run) used in this thesis.

Chapter 3 has been divided into three sections; Section 3.1 describes the model used for this thesis, Section 3.2 describes the filter applied to produce the ENSO-run and Section 3.3 describes the methods for investigating the impact of ENSO.

3.1 Model description

The Whole Atmosphere Community Climate Model (WACCM) from the National Center for Atmospheric Research (NCAR), Boulder, CO, USA is a comprehensive chemistry-climate model. It has 66 levels that spans the altitude range 0 - 140 *km* (that is the surface to $5.1\text{x}10^{-6}$ *hPa*) and uses predetermined sea surface temperatures (containing observed ENSO variability), observed changes in greenhouse gases and halogen species relevant for stratospheric ozone chemistry (García-Herrera et al. [2006]; Marsh et al. [2013]; Randel et al. [2009]). The horizontal resolution of the model is 1.9^o latitude by 2.5^o longitude (Marsh et al. [2013] and the references therein). Other effects such as chemical effects from volcanic aerosol are included but not their radiative effects. In this study the latest version of WACCM has been used and is described in (Marsh et al. [2013]) and the references therein. The first version of the NCAR Community Earth System Model, CESM1 (hereafter CESM1(WACCM)), is based on the Community Climate System Model (CCSM4) and includes now an atmospheric component that extends in altitude to the lower thermosphere, also referred to as an "high-top" model.

This model allows for simulation of the past and future climate in the attempt of capturing coupling processes between the middle and upper atmosphere, troposphere, cryosphere and ocean. Such physical and chemical processes are essential for describing the dynamics and chemistry in the other atmospheric layers above the troposphere. The recognition of the importance of stratosphere-troposphere coupling had led to numerous high-top models being considered in phase 5 of the Coupled Model Intercomparison Project (CMIP5), see (Marsh et al. [2013] and references therein). From such a model - analysis on the variability in dynamics and the distribution of minor species in the stratosphere and mesosphere can be studied. Other significant improvements over the previous WACCM model is the parameterized gravity waves based upon the occurence of convection and the diagnosis of regions of frontogenesis in the model. Additionally, unresolved orography has been parameterized as a surface stress (turbulent mountain stress -TMS), leading to major improvements in the modelling of frequency of sudden stratospheric warmings (SSWs) in the Northern Hemisphere, see (Marsh et al. [2013] and references therein).

Simulations of CESM1(WACCM) has been conducted as part of the phase 5 of the Coupled Model Intercomparison Project, CMIP5, including the active ocean and sea ice components with a nominal latitude-longitude resolution of 1^o as in the CCSM4 simulations. The Version 4 of WACCM represents the atmosphere and is a superset of the Community Atmospheric Model version 4 (CAM4) and includes also all of the physical parameterizations of that model. An updated parameterization of non-orographic gravity waves generated by frontal system and convection and a surface stress due to unresolved topography are also included. The CESM1(WACCM) also includes the QBO, which has been obtained by relaxing equatorial zonal winds between 86 and 4 *hPa* to observed interannual variability. (Marsh et al. [2013] and references therein) but instead of being fixed in either the eastward and westward phase as in Baldwin et al. [2001], the QBO phase varies in in time with approximately a period of 28 months (Marsh et al. [2013] and references therein). This method should however be treated

with caution due to the risk of trends in the region opon relaxation getting damped (Marsh et al. [2013]).

The atmospheric component is essentially the same as that used in the specified SST simulations used in the Chemistry Climate Model Validation 2 (CCMVal2) project. The model's chemistry module is based on version 3 of the Model for Ozone and Related Chemical Tracers. This module contains the species Ox, NOx, HOx, $ClOx$, and $BrOx$ chemical families, along with CH_4 and its degradation products (overall 59 species and 217 gasphase chemical reactions). Additionally, there are 17 heterogeneous reactions on three aerosol types: nitric acid trihydrate, supercooled ternary solution, and water ice. However, this version of WACCM does not include a detailed representation of tropospheric chemistry beyond CH_4 and CO oxidation. As in CCMVal 2, heating from stratospheric volcanic aerosols are computed explicitely (Marsh et al. [2013] and references therein). WACCM specifically encompasses the radiative transfer of carbon dioxide (CO_2), methane (CH_4), nitrous oxide (N_2O) and two halogens: $CFC-11$ and $CFC-12$.

3.2 Approach

The separation between the anthropogenic and natural climate variations is important in climate research. Three sources of natural variations needs to be considered. The first source arises from changes in external radiative forcing affiliated with insolation changes and volcanic eruptions. The second source is generated through internal dynamical mechanisms of interconnecting long-term variability in the ocean. The third source is referred to as climate noise and is associated with the incoherent low-frequency imprint of phenomena with shorter time scales. The dominant contributor of climate noise is the ENSO. On interannual scales the ENSO phenomenon is the largest signal in the climate system but has noise on longer scales. The frequency spectrum of the ENSO is defined by a long low-frequency tail, with its irregularity in the occurences, timing and amplitude of the individual warm and cold ENSO events on 50-yr interval possibly leading to considerable 50-yr trends - thus highly unpredictable. This low-frequency tail contributes to the "ENSO-like multi-decadal variability" and trends, which is mostly climate noise (Compo and Sardeshmukh [2010]; Penland and Matrosova [2006]).

3.2.1 Unwanted noise in climate data

In climate studies, Empirical orthogonal function (EOF) analysis is often used to study potential spatial patterns of variability and how they change with time (like the ENSO or the North Atlantic Oscillation - NAO). EOF analysis attempts to find a relatively small number of independent variables, which includes as much of the original information as possible. For instead instead of X grid points each with N values in time, there are X EOF patterns each with N values in time (Bjornsson and Venegas [1997]). The advantages of EOF analysis is the outcome that entails the index time series, which explains the greatest amount of variability (that is the amplitude of a regression map). EOF gives a compact representation of data (EOF patterns) and time series that are linearly independent, as well as being a convenient method for characterizing dominant spatial patterns of variability. However, there are some disadvantages by the EOF analysis, such as being sensitive to the user's choice of the spatial domain and time period. Also features can be mixed between EOFs if their eigenvalues are similar and the de-

gree of freedom in the time series is too small. There are also no guarantee the EOF pattern has physical meaning (that is EOF analysis can create patterns from "noise"). Therefore, the EOFs should be handled with care.

The typical ocean-atmosphere coupled climate model has been disregarded as Compo and Sardeshmukh [2010] and references therein points out that those models get great errors in representing the tropical variability associated with the ENSO. Many previous studies have addressed the difficulties on the methods on how to estimate the ENSO related variations from climate records. One of them, called the ENSO-filter performed by (Compo and Sardeshmukh [2010]) by will be presented in this section. Their method isolates the ENSO-related component of global SST variations on a month-by month basis in the HadISST1 dataset (Rayner et al. [2003]) using an extended version of Penland and Matrosova [2006]'s patterns-based filter technique. The same extended method has also been used in Sandeep et al. [2014] to study the Pacific Walker Circulation in coupled and uncoupled models. The 136-yr (1871-2006) HadISST data set (Rayner et al. [2003]) is a global SST data set in monthly 1^o area grids provided by the Hadley Centre, Met Office.

The removal of the ENSO-related component anomaly fields from the full SST anomaly fields can affect the multidecadal SST variability and longterm SST trends around the globe greatly. The timeseries of the full SST field component has been compared with the removed ENSO-related component (shortly referred to as the ENSO-unrelated component) and is depicted in Figure 3.2. In Figure 3.2, the black curve shows the globally averaged 10-yr running mean SST anomalies in the HadISST dataset, while the red curve shows the same series after the removal of the ENSO-related components. The adjustment shows noteworthy details throughtout the time series. By a trend of $\sim 0.05\ Kdecade^{-1}$ the originally time series (black curve) for 1871-2006 is being coherent with the estimate by Rayner et al. [2003]. The ENSO-unrelated component (red curve) gives a reduced trend to $\sim 0.03\ Kdecade^{-1}$.

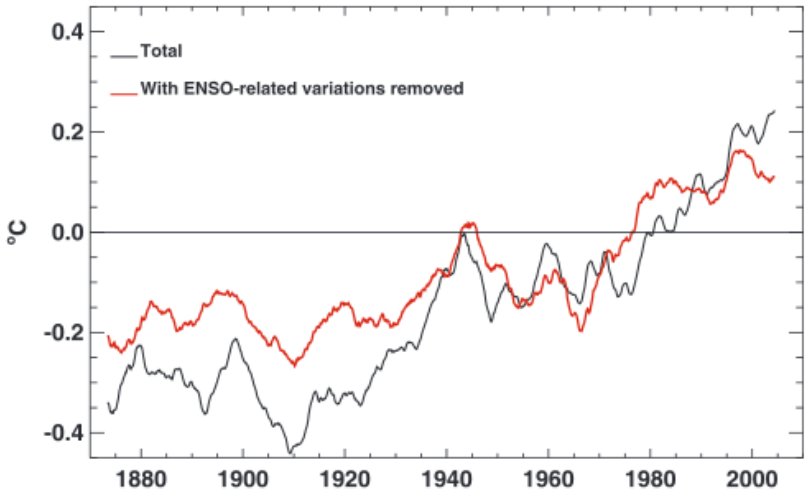

Figure 3.2: Timeseries of the global ocean average surface temperature anomaly (black curve) and its ENSO-unrelated component determined using the ENSO patterns filter (red curve). A 10-yr running mean has been applied to both series. Anomalies are relative to a 1949-2004 climatology. Figure courtesy by Compo and Sardeshmukh [2010].

3.2.2 Dynamical ENSO-filter

This multi-pattern filter (Compo and Sardeshmukh [2010]; Penland and Magorian [1993]; Penland and Sardeshmukh [1995]; Solomon and Newman [2012]) is based on the observed dynamic evolution of ENSO events. They state that identifying ENSO-related variations by regressing on any single ENSO index is problematic. Furthermore, ENSO should not be looked on as one or two numbers but rather as an evolving dynamical process. They identify the ENSO-related SST variations with the projection on the four most important dynamical SST eigenmodes involved in the growth and decay of ENSO events over several seasons. While the statistics associated with ENSO may have changed, the dynamics of ENSO do not appear to have changed (Compo and Sardeshmukh [2010]). The questions is how the ENSO-related variations will be identified. The tropical SST state vector can be presented as

$$\mathbf{x}(t) = \mathbf{x}_e(t) + \mathbf{x}_n(t) \tag{3.1}$$

where $\mathbf{x}_e(t)$ is the ENSO part and $\mathbf{x}_n(t)$ is the non-ENSO part. The rest of the climate state vector can be written as

$$\mathbf{y}(t) = \mathbf{y}_e(t) + \mathbf{y}_n(t) \approx \mathbf{A}\mathbf{x}_e(t) + \mathbf{y}_n(t) \tag{3.2}$$

The reason for the approximation in Equation 3.2 is because $\mathbf{x}_e$ is not necessarily orthogonal to $\mathbf{x}_n$, nor is $\mathbf{y}_e$ to $\mathbf{y}_n$. Yet almost all previous studies have assumed orthogonality even though there is no physical reason to do so. In the absence of preconceptions of the system and only involvement of observations, the dynamical system may be reduced to this simplified system for tropical SSTs in a linear system driven Gaussian white noise.

$$\frac{d\mathbf{x}(t)}{dt} = \mathbf{L}\mathbf{X}(t) + \zeta(t) \tag{3.3}$$

where $\mathbf{L}$ is a deterministic feedback matrix, $\mathbf{x}$ only contains tropical SSTs, and $\zeta(t)$ is the Gaussian white noise (Penland and Sardeshmukh [1995]).

The ENSO pattern filter (EPF) determines the ENSO-related portion of $\mathbf{x}_e(t)$ of tropical SST anomaly fields as $\mathbf{x}_e(t) = \Sigma\alpha_k(t)\mathbf{U_k}$, where $\mathbf{U_k}$ is a particular subset of the eigenmodes of the matrix $\mathbf{L}$ in the linear model (Compo and Sardeshmukh [2010]; Penland and Sardeshmukh [1995]; Solomon and Newman [2012]). The likely forward solution of Equation 3.3 at time t + τ is then

$$\mathbf{x}(t+\tau) = exp(\mathbf{L}+\tau)\mathbf{x}(t) + \varepsilon = \mathbf{G}(\tau)\mathbf{x}(t) + \varepsilon \tag{3.4}$$

where $\mathbf{G}(\tau)$ is $exp(\mathbf{L}+\tau)$. Solution 3.4 describes the tropical SST evolution over several seasons. A linear inverse model can be constructed from estimating $\mathbf{L}$ from data, using the observed lag-covariance matrices $\mathbf{C}(\tau) = \left\langle\ \mathbf{x}(t+\tau)\mathbf{x}(t)^T\ \right\rangle$ at two lags, $\tau = 0$ and $\tau = \tau_0$.

$$\mathbf{L} = \frac{1}{\tau_0} ln\{\mathbf{C}(\tau_0)\mathbf{C}(O)^{-1}\} \tag{3.5}$$

Besides the fact that $\mathbf{L}$ is stable (that is its eigenvalues all have negative real parts), the matrix itself is also non-normal. This means hat its eigenvectors are non-orthogonal because of as-symmetries in the physical system. Then the projection of $\mathbf{x}$ on ϕ_1 tracks projection of $\mathbf{x}$ on ψ_1 7 months later which can be used to predict $\mathbf{x}$ 7 months later. Penland and Matrosova [2006] define the ENSO-related part $\mathbf{x}_e(t)$ of $\mathbf{x}(t)$ not in terms of any index but as a stochastically driven dynamical process (Compo and Sardeshmukh [2010]):

$$\mathbf{x}_e(t+\tau) = exp(\mathbf{L_e}\tau\mathbf{x_e}(t)) + \varepsilon_e \tag{3.6}$$

By doing this Equation 3.6 evolves in an 'ENSO-relevant' dynamical eigenmode subspace of 3.4, where

$$\mathbf{L_e} = \Sigma_i(\sigma_i + i\omega_i)\mathbf{u}_i\mathbf{v}_i^T \tag{3.7}$$

The summation is only over those eigenvectors of $\mathbf{L}$ that results most to the optimal original pattern ϕ_1 associated with ENSO development.

3.3 Methods

This section gives an overview on methods that are often used to study the ENSO phenomena, such as different indices that will be introduced in Section 3.3.1. In Section 3.3.2 the methods used by García-Herrera et al. [2006] has been described.

3.3.1 ENSO related indexes

The aim of these studies is to describe the ENSO signal by analysing the atmospheric temperatures with a focus on the stratosphere and its connection with the troposphere. In the recent decades the importance of the ENSO effects both in the tropics and the extratropics has caught the interest of many authors ([Butler et al., 2014; Calvo et al., 2008; García-Herrera et al., 2006; Li and Lau, 2012]). This subsection will give a brief overview over the possible indices proposed to monitor the ENSO (García-Herrera et al. [2006]; Li et al. [2013]; Randel et al. [2009]). The normally chosen region to study the ENSO is over the region between the longitudes 120^oW and 170^oW and the latitudes 5^oS and 5^oN as shown in Figure 3.3.

3.3.1.1 Niño SST anomaly index (N3.4)

One method is to use the sea surface temperature (SST) index, which is calculated by averaging monthly SST over the selected region in the tropical eastern Pacific, that is the Niño 3.4 SST (see Figure 3.3 for illustration). Positive/negative values are associated with El Niño/La Niña episodes. However, this parameter is not considered as reliable as it only takes account on one variable.

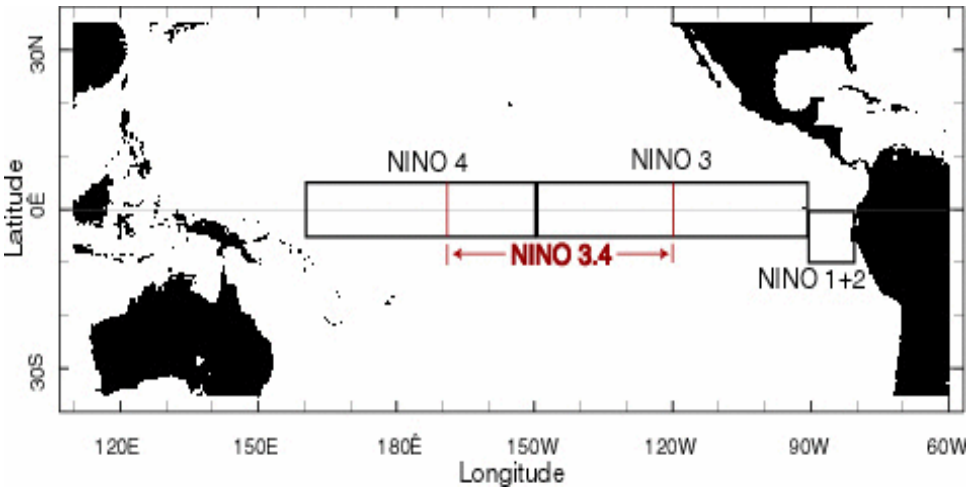

Figure 3.3: Niño3.4 region (120^{o}W -170^{o}W, 5^{o}N-5^{o}S): This region in the tropical Pacific is referred to as the "equatorial cold tongue" by scientists, that is a band of cold water extending along the equator from the coast of South America to the central Pacific Ocean. Significant anomalies from the average sea surface temperatures in this region is of critically importancy of determining major shifts in in the pattern of tropical rainfall, which affects the jet streams and patterns of temperature and precipitation globally.

3.3.1.2 Southern oscillation index (SOI)

There are several ways to describe the ENSO - the phenomenon is often described by the Southern Oscillation Index (SOI), which is based on the pressure difference between Tahiti and Darwin, Australia, as briefly mentioned in Section 2.1.2. The SOI measures the large-scale fluctuations in air pressure occuring between the eastern and western tropical Pacific, that is the behaviour of the Southern Oscillation during El Niño and La Niña episodes. The negative values of SOI means below-normal air pressure in Tahiti and above-normal air pressure at Darwin and vice versa for positive values of SOI. Sustained periods of negative (positive) SOI values coincides with the unusual warm (cold) water covering the eastern tropical Pacific, being in phase with El Niño (La Niña) episodes. For more details about this index, see the page `http://cpc.noaa.gov/products/analysis_monitoring/ensocycle/soi.shtml`. Similar to N3.4, SOI uses one parameter - the sea level pressure difference.

3.3.1.3 Multivariate ENSO index (MEI)

Other ways to study the ENSO variability can be done by using the Multivariate ENSO index (MEI) from the NOAA Climate Diagnostics Center, see the page `http://www.esrl.noaa.gov/pds/enso/mei/table.html` for more details. MEI is a more robust index compared to the indices mentioned above. The MEI combines analysis of multiple meteorological and oceanographic components and is therefore regarded as the most comprehensive index for monitoring ENSO. The MEI is defined at the first seasonally varying principal component of six atmosphere-ocean variable fields, that is sea level pressure (P), zonal and meridional components of the surface wind (U,V), sea surface temperature (SST) and cloudiness from the International Comprehensive Ocean-Atmosphere Data Set (ICOADS).

The reason for this index being a better representative is because it provides a more complete and flexible description of the ENSO phenomenon than the single variable indices such as the SOI or Niño 3.4 SST. In comparison to the SOI and Niño 3.4 SST regions the MEI is the only index that allows for spatial variations of its key features within the seasonal cycle. Additionally, the MEI is less vulnerable to errors than single variable indices (Wolter and Timlin [2011]). This index is a calculated dataset that illustrates the timing and magnitude of the ENSO events, where negative values represent the cold ENSO phase and positive values represent the warm ENSO phase (Calvo et al. [2008]; García-Herrera et al. [2006]; Wolter and Timlin [2011]).

3.3.2 Composite differences of the strongest ENSO events

The approach here is the same as in García-Herrera et al. [2006], where composite differences of the temperatures between the strongest El Niño and La Niña months events during the period 1979-1999 have been computed (see Table 3.1) from a previous version of WACCM (WACCM1b). Their study has been both a motivation and a guideline to study the propagation of the ENSO signal in this thesis. Another important aspect is that their analysis is based on a control-run consisting of observed monthly data including all variabilities, whereas in our study both a control-run (CTRL-run) and a only ENSO-related run (ENSO-run) were available. Thereby giving us the opportunity to perform analysis on the latter where unwanted noise has been removed and explore other aspects that might have been hidden due to noise in the CTRl-run.

A composite map is the average of the anomalies (mean - total mean) of variables from the reanalysis data. The composite of ENSO warm and cold means are simply just the average of those anomalies. Calvo et al. [2008]; García-Herrera et al. [2006] use this kind of map for studying the atmospheric temperatures by taking the composite differences of temperature anomalies between the warmest and coldest ENSO events, see Table 3.1. The events have been chosen whenever this index exceeds standard deviations of 1.2. All the chosen events peaks in late fall-early winter, except for the warm ENSO event in August 1988. The reason for this exemption is to avoid misleading interpretation during the data analysis stage, where the stratospheric dynamics were strongly modified by the seasonal cycle (Calvo et al. [2008]; García-Herrera et al. [2006]). In the composite analysis month 0 is referred to as the month in which all the ENSO events reach their maximum N3.4 index value. Monthly temperature data from CESM1(WACCM) has been preprocessed to eliminate the annual cycle and to remove linear trends. Additionally, a 1-2-1 filter has been applied to smooth short-period fluctuations, same as in García-Herrera et al. [2006].

Date		***N3.4 Value***
	Warm ENSO events	
January 1983		2.74
January 1992		1.82
December 1994		1.32
November 1997		2.76
	Cold ENSO events	
December 1984		-1.21
November 1988		-1.91
December 1998		-1.51

Table 3.1: Central Month and its corresponding N3.4 value for the warmest and coldest ENSO events of interest. Table courtesy by [Calvo et al., 2008; García-Herrera et al., 2006].

Figure 3.4 shows the composite differences (El Niño minus La Niña events) for atmospheric temperature anomalies obtained from WACCM, in a longitude-height domain at 40^{o}N (see García-Herrera et al. [2006] for details about the WACCM version (WACCM1b) used in their studies). These latitudes represent the middle latitudes in the NH, as discussed in Section 2.4. The characteristic patterns of ultralong Rossby waves can be observed and as expected they tilt upward with height. Their results that the most significant anomalies can be observed to up to 35-40 *km*.

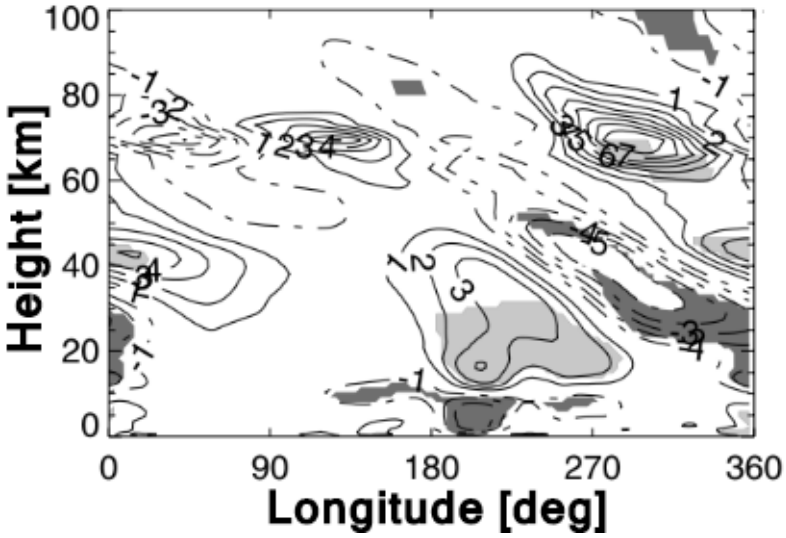

Figure 3.4: Composite differences by (warm-cold events) of temperature anomalies in longitude-height plane. Solid (dashed) lines denote positive (negative) anomalies. Contour interval is $1^{o}C$ and the height is in *km*. Shadowed regions indicate statistically significant anomalies at the 95 % confidence level. Light (dark) gray indicates positive (negative) significant anomalies. Figure courtesy García-Herrera et al. [2006].

In similar way for the temperature, the EP flux differences between composites of warm and cold ENSO events have been calculated from the ENSO-run output variables. Our model results show distinct upward flux differences at higher latitudes of the NH after an El Niño event.

Study by García-Herrera et al. [2006] showed similar results for two models, the Whole Atmosphere Community Climate Model (WACCM1b) and the Middle Atmosphere ECHAM5 (MAECHAM5) (Manzini et al. [2006]). The upward vertical flux departure in the NHfor WACCM3 is also shown in study by Calvo et al. [2008]. However, there are considerable differences from those of WACCM1b. In general, there appear to be significant differences as to even the fundamental features of the ENSO responses related to the EP-fluxes. The same procedure was again used to study the residual circulation and tracer transport.

In the very early stage of this project, correlations and significant plots against the MEI index for different parameters such as the temperature, zonal mean zonal wind, methane and ozone were made. Additionally, seasonal lags against the same index were also plotted. However, it turned out that our approach was not comparable to the composite maps made later on, where the chosen events were picked with respect to their N3.4 index. Thus when we tried to find connections between the correlation and composite plots, patterns were not easy to detect and we choose not to include those statistics plots. Though we kept the overview over the ENSO related indices as later on in the discussion, a few papers using these indices will be mentioned .

CHAPTER 4

Results and Discussion

In this chapter the results from the ENSO-run of the CESM1 (WACCM) model will be presented. The following topics will be explored: the vertical propagation of the planetary waves into the stratosphere, the dissipation of the wave amplitude, the deceleration of the westerlies, the induction on the residual circulation and the distribution of chemical tracers. The similarities and differences with García-Herrera et al. [2006] will also be highlighted. This chapter has been divided into the following sections: Section 4.1 reviews the climatology relevant for the aforementioned topics; Section 4.2 reviews the modulation of the ENSO signal onto the middle atmosphere; Section 4.3 addresses how the modified residual circulation affects the tracer distribution.

4.1 Boreal winter climatology for the period 1955 - 2001

In this section, observed NH winter climatology of temperature, the zonal mean wind, the EP-flux vectors, the divergence of the EP-flux vector, the residual mean circulation and the chemical tracers will be presented and discussed. Climatology plots will be used later on as references when studying their ENSO-related anomalies.

4.1.1 Distribution of zonal temperature and mean wind

Figure 4.1a shows the vertical temperature structure of the middle atmosphere during NH wintertime. The temperature and location of the tropopause varies because of the dependency on the latitude and season. At the equator the mean tropopause pressure is around 50 *hPa* (equivalent to 18 - 20 *km* of altitude) with a corresponding temperature of about 190K, while in the polar regions the pressure level is less than 200 *hPa* (about 10 *km*) and the temperature is approximately 210K. Following the tropopause is the stratosphere with temperature increasing with height and with a maximum of about 260K at the stratopause (pressure near 1 *hPa* and altitude of about 50 *km*). Above this layer lies the mesosphere with decreasing temperature with pressure down to 0.01 *hPa* (up to 85 *km*) and the mesopause as its upper boundary.

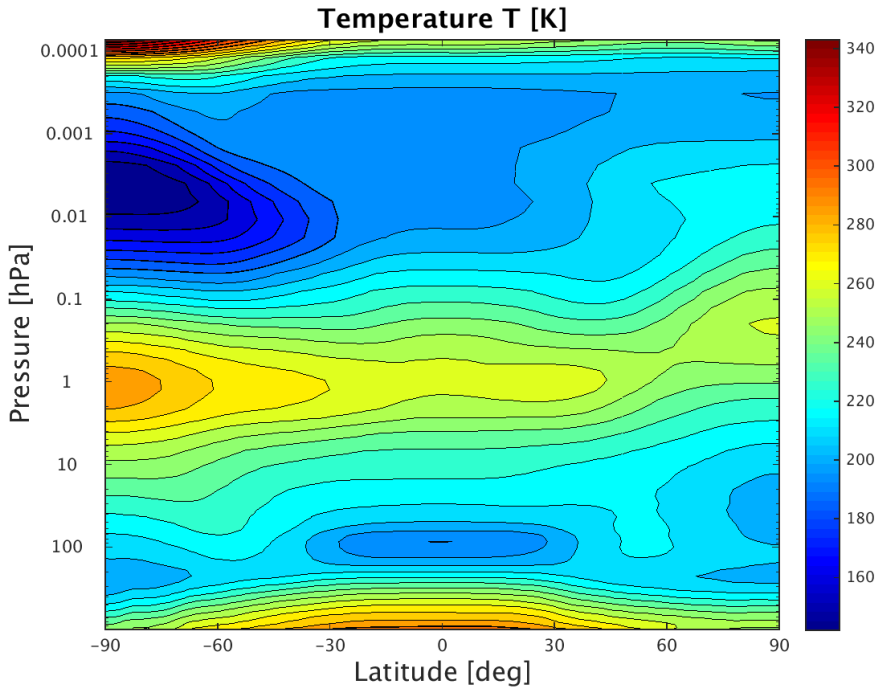

(a)

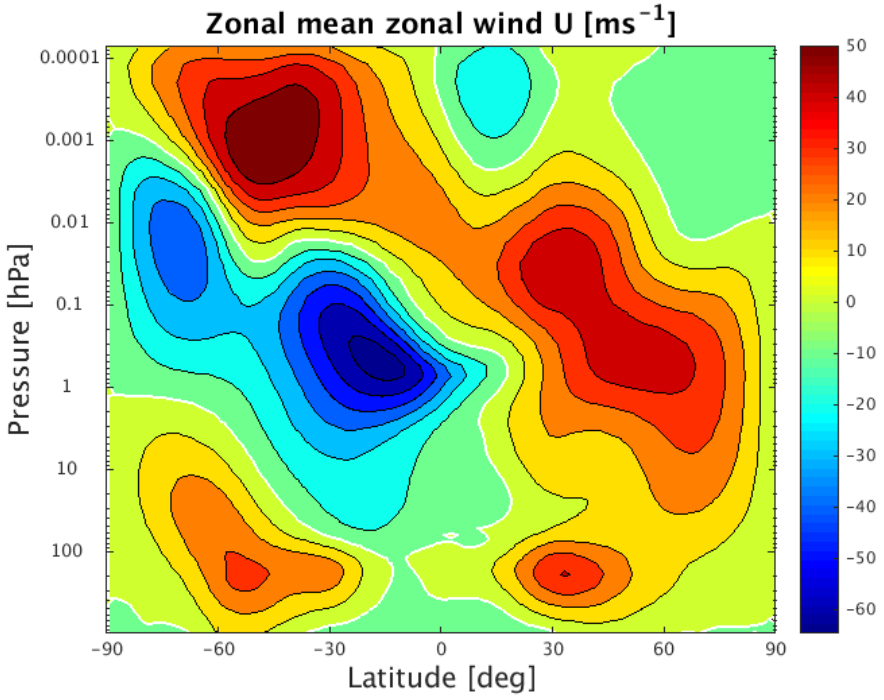

(b)

Figure 4.1: Winter climatology (December-January-February) of a) the temperature (K) and b) the zonal mean zonal wind (ms^{-1}) as function of latitude and pressure for the period 1955-2001. Positive (negative) values denote westerlies (easterlies). For figure b) thin white line marks the boundary line between easterlies and westerlies. Contour interval is 20K in figure a), and 10 ms^{-1} in figure b).

In the thermosphere, the temperature increases with height due to absorption of ultraviolet light. Figure 4.1b shows the features of the zonally averaged zonal wind distribution for the averaged winter seasons. The main features observed are a westerly jet in the winter hemisphere and an easterly jet in the summer hemisphere in the stratosphere, respectively with wind speeds of 50 ms^{-1} and 60 ms^{-1}. The tropospheric jets can be seen for both hemispheres in the subtropics. The winds near the ground are much weaker compared to the above layer. At the core of the subtropical jets, stronger winds can be found. The strongest wind are located near 30 ^{o} latitude in the winter hemisphere near the 200 *hPa* level with an averaged speed of around 30 ms^{-1}. In the summer hemisphere, a weaker jet is located near 50 ^{o} with a speed of about 25 ms^{-1}. During the northern winter, much weaker easterlies are observed. Figure 4.1a and 4.1b coincides well with the literature such as in Brasseur et al. [1999]; Holton and Hakim [2012].

4.1.2 Dissipation of wave amplitude

The Eliassen Palm-vector (EP-flux vector) is considered as a measure of the propagation of Rossby wave activity (Section 2.3.3). The vertical propagation of waves into the stratosphere are in accordance with the wind regimes where winds are westerly during the NH winter (Figure 4.1b). Figure 4.2 shows the winter distribution of the EP-flux vector. For later comparisons of the EP-flux, the same vertical range has been choosen as in García-Herrera et al. [2006] – between 50 - 0.1 *hPa* (or 20 - 60 *km*). The upward propagation of Rossby waves into the NH middle atmosphere is visible in Figure 4.2.

Figure 4.2a reflects the distribution for $\mathcal{F}_{\mathbf{y}}$ (Equation 2.5) and the behaviour of the momentum flux when being affected by atmospheric waves. A strong northward flow for $\mathcal{F}_{\mathbf{y}}$ can be observed at mid-latitudes with the highest values centered around 40 - 50^{o}N in the lower stratosphere extending up to the lower mesosphere. Between 60 - 80 ^{o}N a weak southward flow can be detected in the lower stratosphere. In Figure 4.2b a strong intense upward flow for $\mathcal{F}_{\mathbf{z}}$ can be observed as well with the most significant values centered around 50 - 70^{o}N from the lower stratosphere up to the middle mesosphere. Respectively for Figure 4.2a (4.2b) a southward (upward) propagation can be observed in the SH.

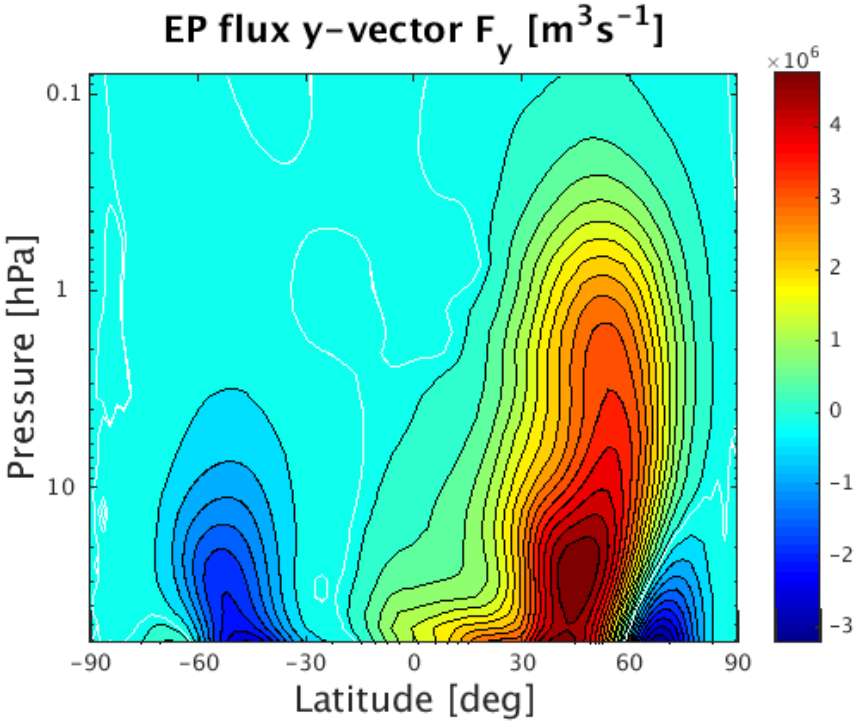

(a) $\mathcal{F}_y$

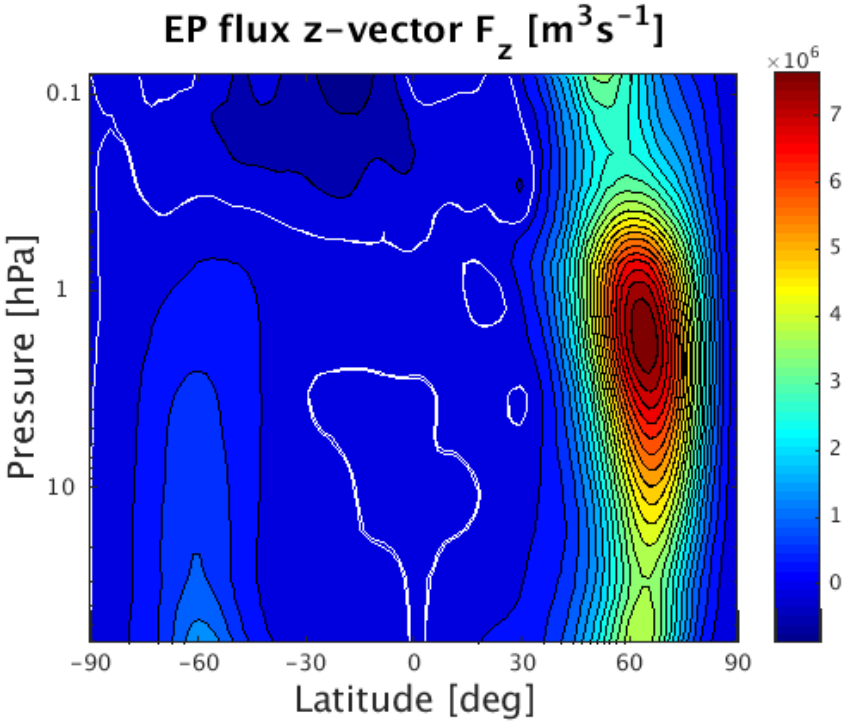

(b) $\mathcal{F}_z$

Figure 4.2: Winter climatology (December-January-February) of the EP-flux vector as function of latitude and pressure for the period 1955-2001. The vectors have been scaled by the inverse density to make them more apparent in the stratosphere. For the EP-flux y-vector: positive (negative) values indicate northward (southward) motion. For the EP-flux z-vector: positive (negative) values indicate upward (downward) motion. Units are $m^3 s^{-1}$.

The divergence of the EP-flux vector is an important term to understand the effect of eddies and waves on the zonal mean state of the atmosphere. This term appears as the reflection of the wave activity as illustrated in Figure 4.3. Negative values for the divergence of the EP-flux ($\mathcal{F} < 0$) indicate convergence zones, which implies the deceleration of the westerlies. It is explained by the deposition of easterly momentum by Rossby waves. Therefore weaker vortex is observed in the NH winter in contrast to the SH winter. Positive values of the divergence of the EP-flux ($\mathcal{F} > 0$) indicate divergence zones which implies to the acceleration of the westerlies. From the above interpretation of the wave propagation in Figure 4.2 and Figure 4.3 we concluded that the zonal mean zonal flow accelerates in regions where the EP-flux vector diverges, and decelerates in regions where the EP-flux vector converges. The next logical step is to look into the residual circulation with its uplifting in the tropics and descent in the polar regions.

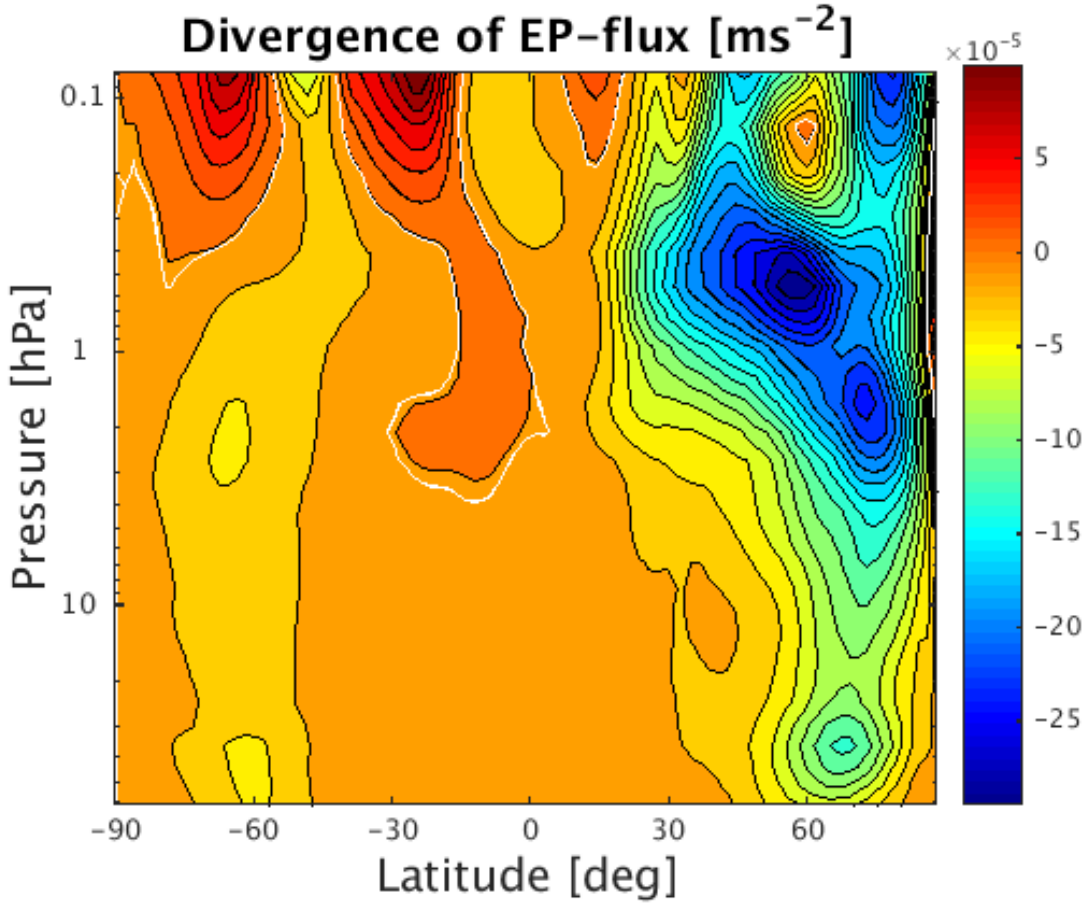

Figure 4.3: Winter climatology (December-January-February) as function of latitude and pressure of the EP-flux divergence for the period 1955-2001. Positive (negative) values indicate regions of divergence (convergence). Thin white line denotes boundary between positive and negative values. Units are ms^{-2}.

4.1.3 The residual circulation

One way to analyse the zonal mean circulation is to use the tranformed Eulerian mean (TEM, see equations described in Section 2.3.2). This formulation provides a clearer diagnosis of

the eddy forcing and gives a more direct picture of the transport processes in the meridional plane. There are tendencies of strong cancellation between the eddy flux heat convergence and adiabatic cooling (Brasseur et al. [1999, chapter 2], Holton and Hakim [2012, chapter 10]), meanwhile the diabatic term is a small residual. The increase of potential temperature due to diabatic heating, leads to the rise of an air parcel to higher altitudes. Thus the residual mean circulation $(\overline{V}^*, \overline{W}^*)$ is associated with diabatic processes, that are directly related to the mean meridional mass flow. The TEM formulation (Equation 2.4) points out that the eddy heat and momentum flux are dependent of each other, driving the changes in the zonal mean circulation but only when combined with the divergence of EP-flux. In conclusion, the fundamental effect of the eddies is to exert a zonal force.

Figure 4.4 shows the winter climatology of the meridional and vertical TEM circulation for the analysed period. For Figure 4.4a a northward motion is governing the mesosphere with the strongest values in the upper mesopshere. Southward motion can also be observed with the weakest values in the stratosphere and the strongest in the thermosphere. In Figure 4.4b, the circulation of $\overline{W}^*$ is stronger in the SH summer than in the NH winter. This is as expected since the gravity wave drag is stronger in the SH. In the mesosphere, a single circulation cell is dominating the residual circulation with upward motion in the summer polar region, meridional drift from the summer to the winter hemisphere is observed and subsidence in the winter polar region is visible. The values in Figure 4.4a are, as expected, greater than in Figure 4.4b.

The residual circulation is driven by the eddies but in contrast to the stratosphere where the planetary waves are dominating the eddy activity, the internal gravity waves are dominating the eddies in the mesosphere. The overall picture on the climatology of the residual circulation is as follows:

- An ascent in the tropics with descent in the polar region is observed in the stratosphere.
- An ascent in the south pole region with a meridional drift from the summer to then winter hemisphere followed by a descent in the north pole region.

The overall movement in Figure 4.4 fits the schematic of the BDC shown in Figure 2.4 and discussion presented in Section 2.3.1. Another important aspect is that this vertical circulation is closed in the lower stratosphere by a poleward meridional drift balanced by the EP-flux convergence (Holton and Hakim [2012, chapter 12]).

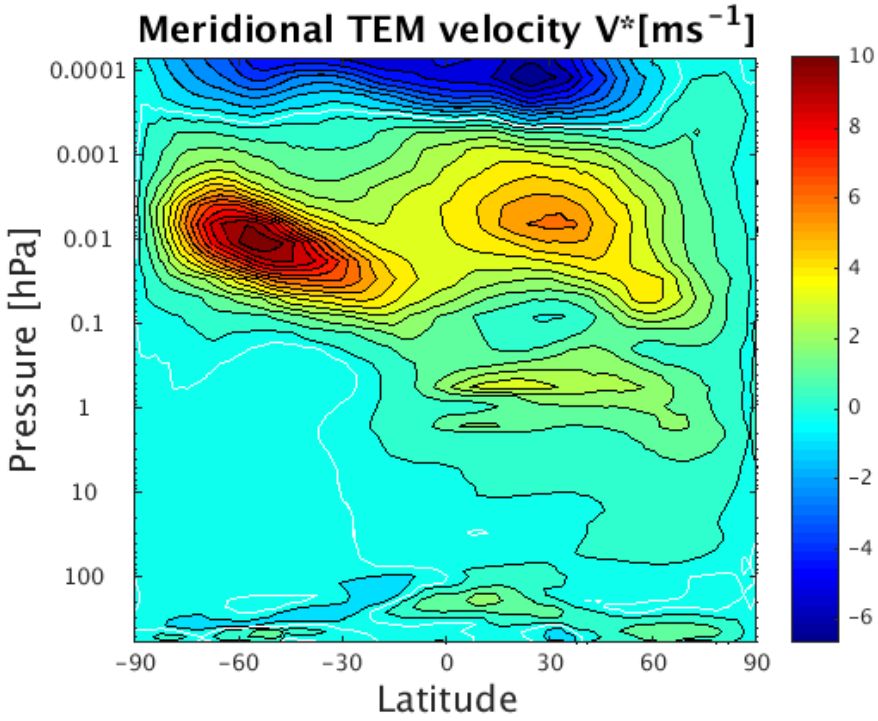

(a) $\overline{V}^*$

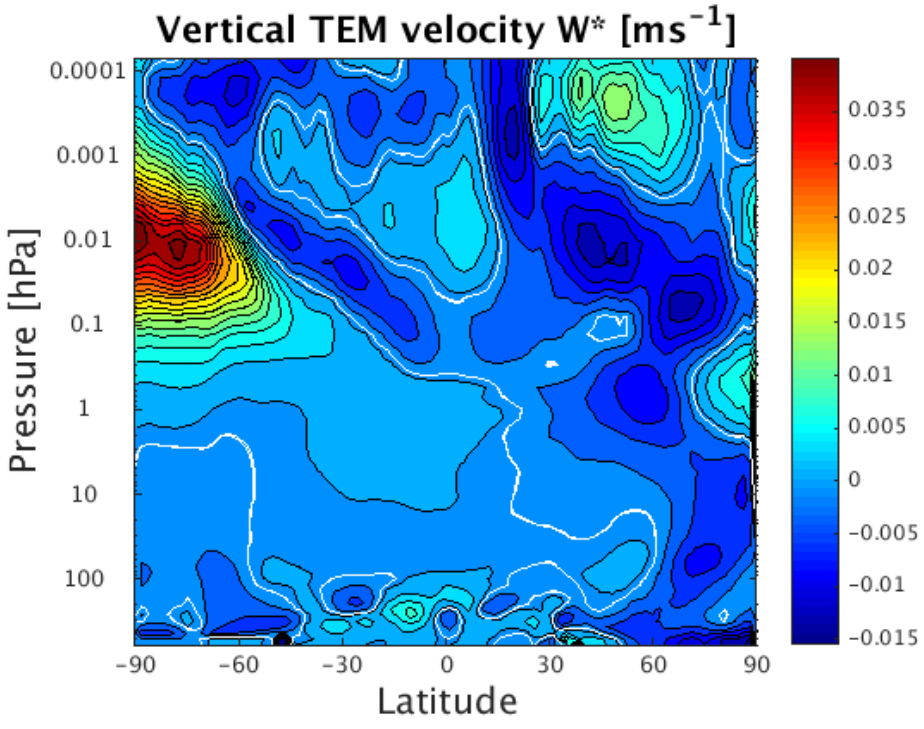

(b) $\overline{W}^*$

Figure 4.4: Winter climatology (December-January-February) of the residual circulation (V*,W*) as function of latitude and pressure for the period 1955-2001. For a) the meridional TEM velocity, $\overline{V}^*$: positive (negative) values denote northward (southward) motion, wheras for b) the vertical meridional TEM, $\overline{W}^*$, positive (negative) values denotes upward (downward) motion. Thin white line denotes boundary between positive and negative values. Units are ms^{-1}.

4.1.4 Distribution of N_2O, CH_4 and O_3

The presented methodologies in this chapter so far have been included to increase our understanding of the dynamical concepts and transport that are essential in the stratosphere. The TEM circulation (Section 2.3.2) is a robust approximation to the BDC and explains the distribution of the different tracers. The stratospheric chemistry is to a large degree governed by ozone (which is a very active tracer and a product of solar radiation induced photochemistry), as well as by the inflow of various chemical compounds from the troposphere (Brasseur et al. [1999]). In addition, the ozone concentration has a great impact on the diabatic heating which may influence both the temperatures and winds. The temperature affects the ozone in the way that it triggers many important reaction rates related to the ozone chemistry. Meanwhile the winds affects the ozone distribution by including other tracers trough transport.

The diabatic heating (Figure 6.2a in Appendix) in the stratosphere is primarily a result from solar radiation absorption by ozone with a maxima of $\sim 14\ Kday^{-1}$ near the summer stratopause. The observed cooling (Figure 6.2b in Appendix) occurs through radiative transfer by CO_2, H_2O and O_3. At the winter pole, cooling is much larger than heating. The reason being that the sinking branch of the meridional circulation cell maintains the temperatures above the radiative equilibrium values (Brasseur et al. [1999]). As stated before, the mean circulation in the stratosphere is primarily governed by atmospheric waves despite of the large diabatic heating. By overcoming the restraints on meridional motion, Rossby waves in the winter hemisphere transport mass poleward. Tracers such as nitrous oxide, methane and ozone with their meridional gradients are efficiently transported.

N_2O is a long-lived anthropogenic greenhouse gas (GHG) and has a global warming potential significantly greater than CO_2. Among the ozone-depleting substances (ODS), emissions of N_2O is currently considered as the largest (Thompson et al. [2013] and references therein). The source of N_2O is the troposphere (where it is a well-mixed gas). Its concentration then gradually decreases with height in the stratosphere due to destruction primarily by photolysis (a process that yields N_2 and O_3). A second destruction pathway is through reactions with excited oxygen atoms which gives NO molecules (Brasseur et al. [1999, chapter 2]). N_2O is a good tracer of the movement of air parcels due to its lifetime (over $\sim$ 100 years at 50 hPa or 20 km) that is much greater than that of atmospheric dynamical processes. On interannual variability, Thompson et al. [2013] found strong correlations between N_2O and the MEI index (mentioned in Section 3.3.1.3).

The distribution of the N_2O is shown in Figure 4.5a. Through the formation of NO, this long-lived GHG plays an important role in the depletion of stratospheric ozone. Increased concentration in the troposphere is due to upwelling movement, and decreased concentration in high latitudes is caused by downwelling movement. Therefore the mean meridional circulation will generate a meridional gradient with higher values found in the tropics (Brasseur et al. [1999]). As seen in Figure 4.5a, the isolines of mixing ratio slope downward from equator to pole. Breaking of Rossby waves causes mixing, and leads to smoothing of latitudinal gradients of mixing ratio. A sharp gradient at high latitudes is an indicator of the edge of the polar vortex (Figure 2.5), however this is not as clear in Figure 4.5a.

A similar distribution than for N_2O can be seen for CH_4. The distribution exhibits the characteristic shape of upward mass transport, that is the upwelling in the tropics and downwelling in the extratropics because of the BDC but smoothed out by quasi-horizontal mixing.

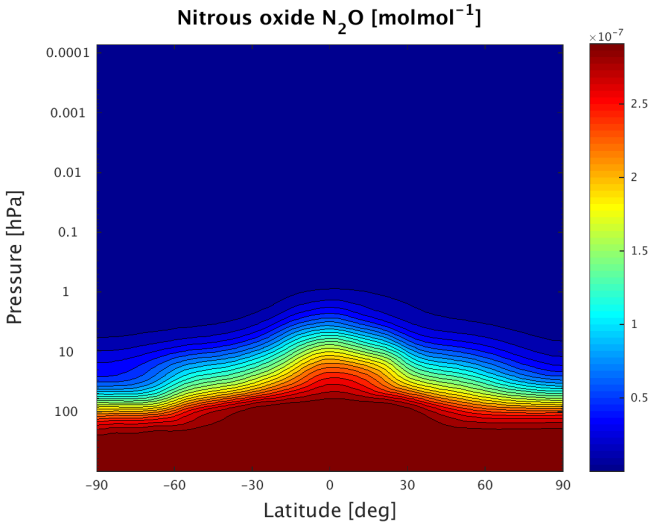

(a)

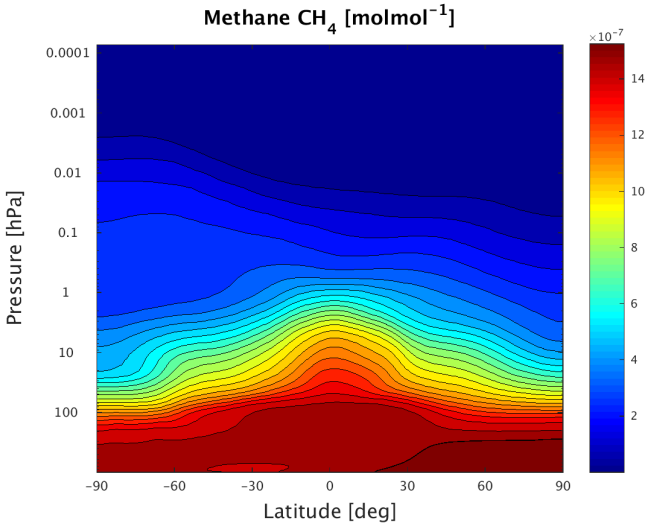

(b)

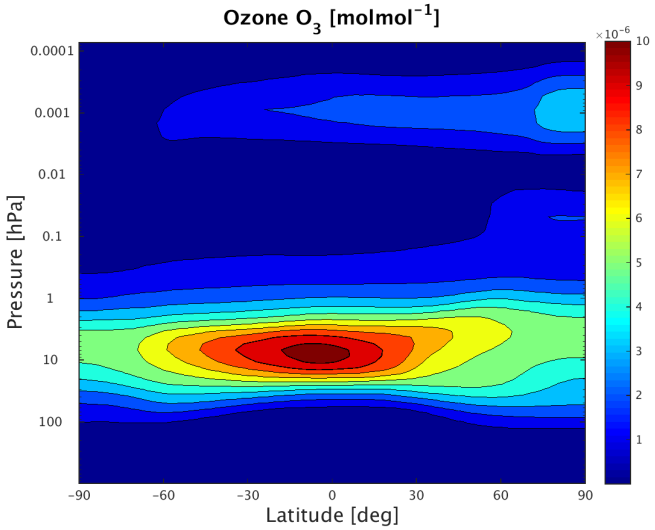

(c)

Figure 4.5: Winter climatology (December-January-February) of the concentrations of N_2O (top) and CH_4 (middle) O_3 (bottom) as function of latitude and pressure for the period 1955-2001. Units are in $molmol^{-1}$.

Depending on their chemical lifetime, these characteristics are approximately the same for all long-lived tracers due to transport, except that the changes in the vertical direction differs (Shepherd [2007]). Methane has its source region in the troposphere and diminishes in the stratosphere due to reaction with OH molecules and oxygen atoms. While high methane air is carried from the tropical lower troposphere into the tropical stratosphere through the ascending branch of BDC, low methane air is carried from the polar upper stratosphere into the polar lower troposphere through the descending branch of the BDC.

Figure 4.5c depicts the distribution of ozone during the NH winter. The tropical stratosphere is the global source of ozone due to its transport out of this region. As expected for Figure 4.5c most ozone production occurs in the tropical stratosphere due to the sun breaking oxygen molecules (O_2) apart and into oxygen atoms (O) which react with other O_2 molecules to create ozone (O_3). But the simplified picture does not tell the whole truth. From observations, most ozone is detected outside the tropics at higher latitudes far away from its original source region. Ozone is indeed primarily produced in the tropical stratosphere but is then transported poleward and downward, which is explained by the BDC and discussed in Section 2.3.1.

4.2 Exploring composite differences of strong ENSO events

In order to study the upward propagation of the ENSO signal and the different processes through which the signal reaches the stratosphere, the ENSO-run from the CESM1(WACCM) model was used. Previous studies primarily used datasets similar to the CTRL-run. In these runs, only the significant ENSO events were highlighted causing the occurrence of other ENSO events to be masked by other variabilities. Through this model run we see different kinds of pattern now that ENSO-related components have been accentuated. The monthly averages for the period 1979 - 2000 were computed in order to do comparisons with earlier work by García-Herrera et al. [2006] on the same period. The composites of the strongest El Niño minus La Niña events for different latitudes have been studied and analysed. The composite analysis displayed here are all for month 0, which is the month where all ENSO events reach their maximum N3.4 value.

As noted in Section 3.3.1, a variety of indices can be used to characterize the ENSO phenomenon but in order to follow the same approach as García-Herrera et al. [2006], we will use the same index, the N3.4 index. Similarly as in that study, warm and cold ENSO events have been chosen whenever their index exceeds a 1.2 standard deviations (Table 3.1). A previous version of WACCM (WACCM1) was used in their results and they chose the latitude of 40^oN as a representative in the longitude-height plane for the composite differences (El Niño minus La Niña). However in our results obtained from the ENSO-run, the latitude 50^oN seems to be a more appropriate representative.

4.2.1 The ENSO signal in the stratosphere

Figure 4.6 displays the composite differences (El Niño minus La Niña) for monthly mean temperature anomalies in the longitude-height plane at latitude 50^oN after an El Niño event. This latitude will be the representative of the NH's middle latitudes. A similar pattern can be observed in Figure 4.6, where the most evident temperature anomalies are found in the troposphere and stratosphere. The temperature anomalies indicates the upward propagation of the

ENSO signal in the direction of the stratosphere due to large-scale Rossby waves during month 0. In the troposphere, patches of negative anomalies can be detected with positive anomalies above the tropopause tilting westward with height, thus displaying this upward propagation. When these waves reach the stratosphere they break and deposit easterly momentum due to the EP-flux convergence.

In Figure 4.6, slightly enhanced temperature anomalies can be seen emerging from the lower stratosphere with values less than $1K$ tilting upwards to the upper stratosphere with values equal to $3K$. These anomalies are then followed by cooling due to the weakened temperature anomalies above, stretching from the lower stratosphere and tilting towards the upper mesosphere with values equal to -4K. Significant anomalies are then observed in the middle mesosphere with the largest values over $5K$, whereas in García-Herrera et al. [2006] the largest values are around $7K$. The somewhat smaller values in the middle atmosphere seem to be confirmed by the upcoming results for the temperature anomalies. In general, a ENSO-like signal can be detected in our results, consistently with what can be presented in García-Herrera et al. [2006]. However, our results seem to have a slightly less slanting look, while on the other hand the anomalies are more widely stretched in their appearance.

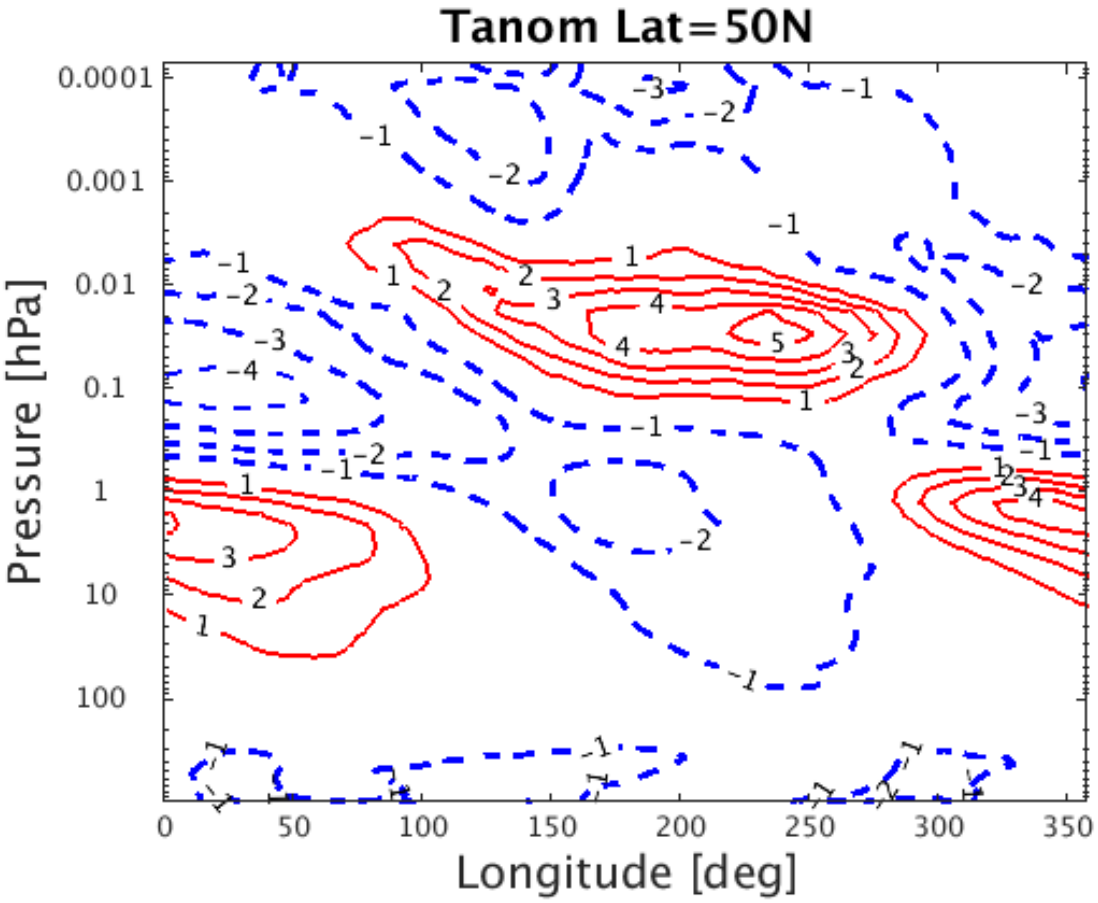

Figure 4.6: Composite differences (El Niño minus La Niña) for the temperature anomalies at latitude 50^{o}N from the CESM1(WACCM) simulation after an El Nino event. Contour interval is $1K$ (zero line is not displayed).

The vertical propagation of Rossby waves is strongly connected to the zonal-wind regimes

(Figure 4.1b). Rossby waves propagate into the stratosphere primarily during the the winter because vertical propagation requires the zonal-wind to be westerly and lower than a certain critical value that depends on the total horizontal wave number (the Charney and Drazin criteria). Therefore in the winter stratosphere, only ultra-long Rossby waves in association with the climatological westerly winds are allowed to propagate into the stratosphere. According to the CD criteria, the NH westerlies favour vertical wave propagation into the middle atmosphere, while SH easterlies prevent wave propagation above 100 *hPa* (or 20 *km*). Thus observations show ENSO events peaking during the boreal winter.

Additionally in Figure 4.6, a significant warming in the tropical middle mesosphere and cooling in the NH polar middle mesosphere can be observed. Study by Sassi et al. [2004] show similar findings were an earlier version of WACCM (WACCM1b) was used. They propose a possible explanation: since the stratospheric westerly winds in the NH weakens during warm ENSO events, the least eastward portion of the upward propagating gravity waves are filtered through the critical level absorption by westerlies (Sassi et al. [2004]). This causes the climatological gravity wave forcing (not shown) in the NH mesosphere to become less westward. This could also explain the outcome in Figure 4.11b where a more eastward anomalous gravity wave drag in the NH mesosphere is observed and thus a cooling occurs.

Being aware of the ENSO-related temperature anomalies dependency on latitude is very important. To ensure a complete overview, the composite differences for a range of latitudes in both hemispheres are presented in Figure 4.7-4.8. By comparing the latitudes, the differences between the hemispheres in the extratropics and within each hemisphere have been highlighted as in García-Herrera et al. [2006]. The ENSO signature changes from being sealed up to 100 *hPa* at tropical latitudes to transition of upward propagation into the middle atmosphere at higher latitudes.

For the tropical regions shown in Figure 4.7a and 4.8a, the ENSO-related anomalies with respect to Rossby waves are confined to the troposphere and lower stratosphere with values less than $1K$. The confinement of the anomalies seems to be in line with García-Herrera et al. [2006] but their anomalies are more significant both in terms of value and upward tilting. In both hemispheres at latitude 20^o the least significant anomalies can be observed (Figure 4.7b and 4.8b). At latitude 40^oN (Figure 4.7c), significant anomalies are observed tilting westward in the stratosphere with the largest values equal to $4K$. Then a zonal band of cooling in the lower mesosphere can be seen with colder temperatures tilting upward into the mesopause. As in Figure 4.6, warmer temperatures in the tropical middle mesosphere are seen. Our results point out that vertical propagation is the most effective at latitudes 40^oN and 50^oN (Figure 4.7c and 4.6 respectively) and becomes less effective towards higher latitudes. For higher latitudes in the NH the significant signal resembles a more zonally symmetric shape (Figure 4.7d).

We have emphasized that the vertical propagation of Rossby waves is strongly connected to the zonal wind regimes. In our selected latitudes for the SH summer (Figure 4.7) we see how the SH easterlies prevent wave propagation above 100 *hPa*. In the tropical region for the zonal mean zonal wind winter climatology (Figure 4.1b), easterlies between 50 *hPa* and to 0.5 *hPa* can be observed. Additionally in this region, low frequency extratropical Rossby waves are present (Andrews et al. [1987]) and are defined by small group- and phase velocity. Under these terms, vertical propagation of waves are prohibited and also more exposed to damping or absorption.

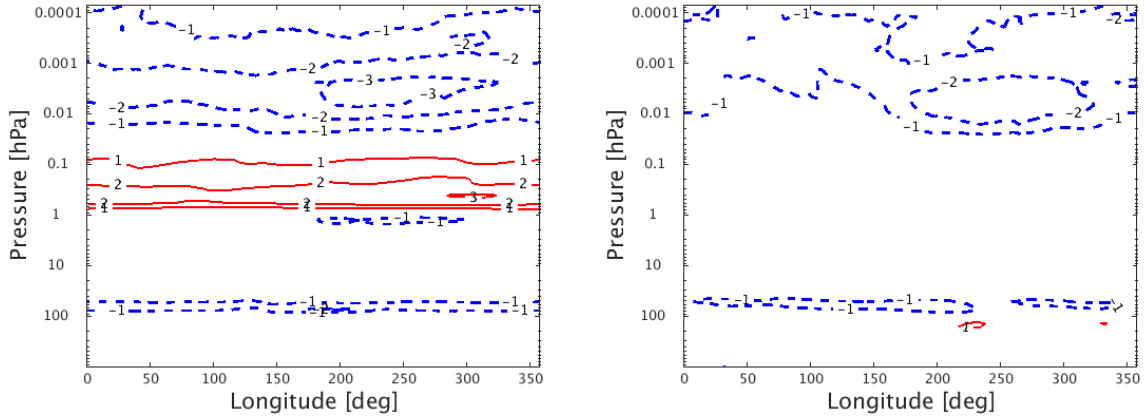

(a) Lat=1^oN

(b) Lat=20^oN

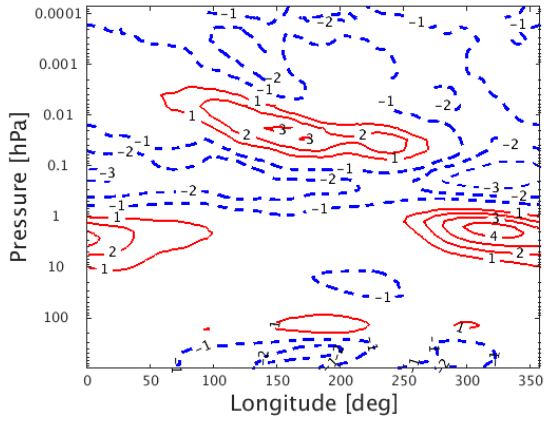

(c) Lat=40^oN

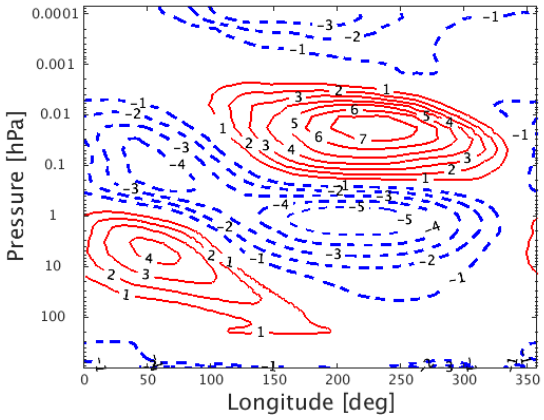

(d) Lat=70^oN

Figure 4.7: Composite differences (El Niño minus La Niña) for the temperature anomalies at different latitudes in the NH after an El Nino event. Contour interval is 1 K. Zero contour has not been displayed.

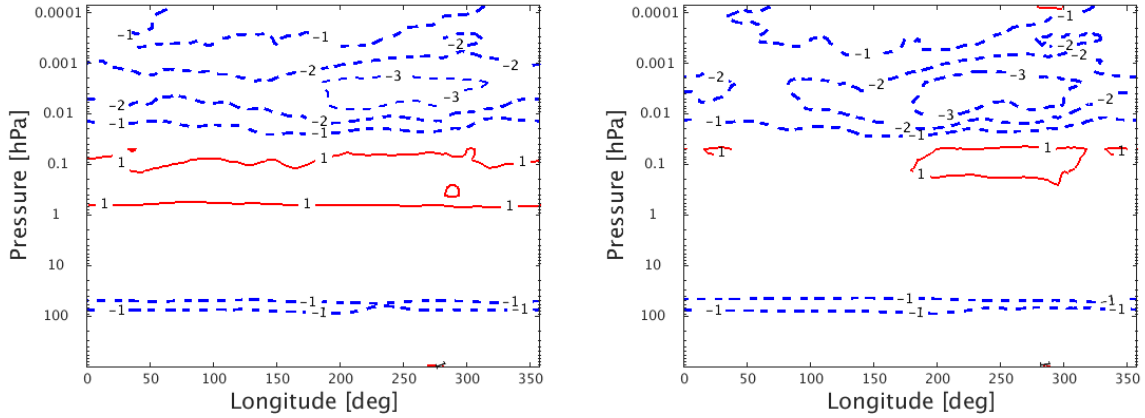

(a) Lat=$10^o S$

(b) Lat=$20^o S$

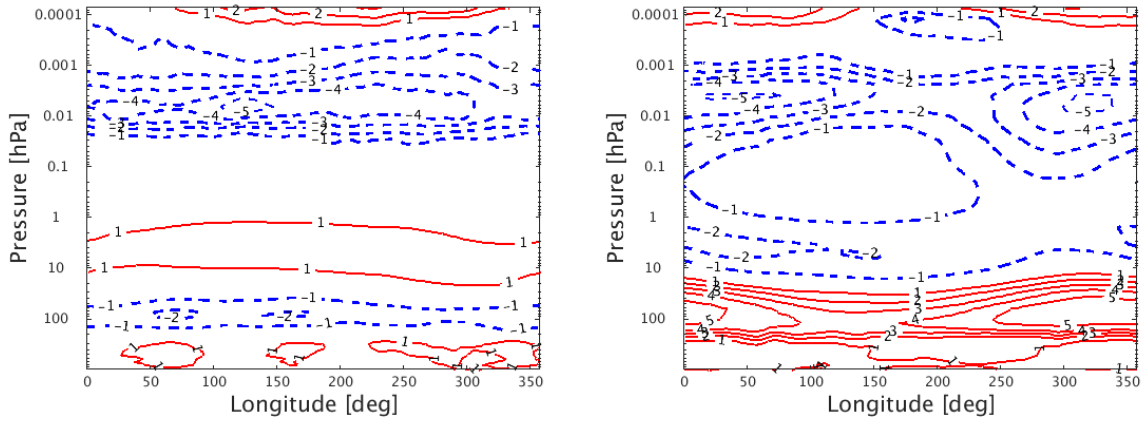

(c) Lat=$40^o S$

(d) Lat=$70^o S$

Figure 4.8: Composite differences (El Niño minus La Niña) for the temperature anomalies at different latitudes in the SH after an El Nino event. Contour interval is 1 K. Zero contour has not been displayed.

We chose the latitude 40^oS as the representative for the middle latitudes in the SH, where a wave-like shape is visible. Figure 4.8c shows the composite differences at 40^oS. Compared to its conterpart in the NH, the propagation into the stratosphere here is less efficient with weaker anomalies up to 100 *hPa*. This is in accordance with the difference in vertical propagation efficiency of the ENSO signal between the SH and NH with respect to the wind regimes. Another interesting observation is what is observed for latitude 70^oS. Figure 4.8d shows that there is a strong warm anomaly in the upper troposphere/lower stratosphere. This is later confirmed again in the zonal mean cross section for the composite differences of the temperature anomalies in Figure 4.9. Since the SH summer has not been our main priority, we have not focused our discussion on the SH anomalies. However, it would be very interesting to understand what causes this strong anomaly. As well as in the previous section, we beleive that future work could further analyse this: looking into their seasonal conditions, figuring if these anomalies occur early in the austral spring, how is the linkage to the O_3... Results in subsequent sections focus on the zonal mean cross sections.

garher06

4.2.2 The zonal analysis of the ENSO signal

The ENSO generates significant anomalies in the zonal field (e.g. Calvo et al. [2008]; García-Herrera et al. [2006]; Sassi et al. [2004]). Extreme ENSO events modify the stratospheric branch of the mean meridional circulation (García-Herrera et al. [2006]), which is reflected in the anomalous patterns in zonal mean temperature and zonal wind. In the NH, westerlies are dominating, extending from the troposphere to the mesosphere, whereas easterlies are observed from the tropics and into the mesosphere in the SH. In addition to the earlier discussion about the CD criteria, we notice that during the NH winter westerlies allow for the vertical propagation of Rossby waves into the middle atmosphere. Meanwhile, for the SH summer, vertical wave propagation is not expected as easterlies inhibit propagation above 50 *hPa*. This is in agreement with our results shown in the previous composite differences as well as in Figure 4.9.

Figure 4.9 depicts the composite differences (El Niño minus La Niña) for the zonal mean temperature anomalies. Previous studies such as (Fernández et al. [2004]; Yulaeva and Wallace [1994]) found a zonally symmetric warming that develops during the mature phase of a warm ENSO event in the tropical troposphere. However, in our result this is not as obvious and instead we observe a weaker warming in the tropical troposphere. In the tropical stratosphere, the negative anomalies observed above 100 *hPa* in Figure 4.7b and Figure 4.8b are also obvious in the zonal mean temperature analysis of Figure 4.9. A weak anomalous warming can be seen in the polar lower stratosphere in the NH, accompanied by cooling from the middle stratosphere to the middle mesosphere and followed by a warming in the upper mesosphere. Study by Li et al. [2013] also show similar findings but the significant anomalies are observed in the middle mesosphere instead, in agreement with previous modelling studies, e.g. García-Herrera et al. [2006].

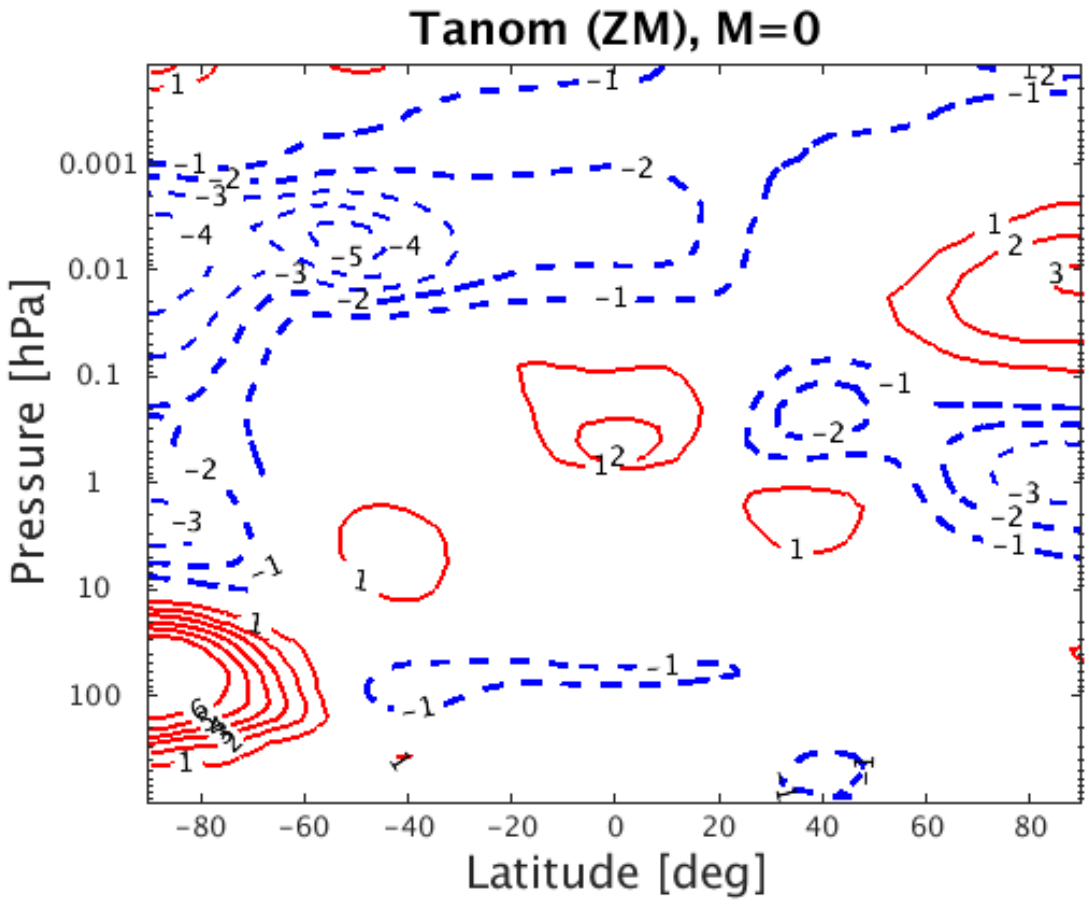

Figure 4.9: Composite differences (El Niño minus La Niña) for the temperature anomalies after an El Nino event. Contour interval is $1K$ (zero line has not been displayed).

A dipolar structure can be observed with negative and positive anomalies situated between 10 and 0.02 *hPa* at high latitudes in the NH. In similar fashion, a second dipole can be found in the polar SH but at lower heights. In the model study of Sassi et al. [2004], these anomalies in the boreal winter were also found but are on the other hand situated between 1 and 0.05 *hPa* with a reversal in sign. According to Manzini et al. [2006]; Sassi et al. [2004], the ENSO-related anomalies are at higher latitudes and are related to warm ENSO events. In the SH, the strong anomaly mentioned in the previous section is also very apparent in the zonal field, covering most of the upper troposphere/lower stratosphere at polar latitudes.

In association with the strong El Niño events, weaker (enhanced) zonal mean zonal winds are observed in the stratosphere (mesosphere) at middle and high latitudes in the winter hemisphere (Figure 4.12). The deceleration of the westerlies is explained by the deposit of easterly momentum (EP-flux convergence) due to the propagation of Rossby waves into the stratosphere (EP-flux). This will be discussed in more details in the following section. These observed anomalous patterns in the zonal mean temperature (Figure 4.6) and zonal wind (Figure 4.12) signal the modification of the stratospheric branch of the mean meridional circulation. This circulation carries air from the tropical lower stratosphere to the polar regions in the winter hemisphere and is forced by the dissipation of the atmospheric waves (Calvo et al. [2008]; García-Herrera et al. [2006]; Li and Lau [2012]). This wave dissipation can either be in the form of thermal dissipation or wave breaking (more details in Section 2.4). Until now, our

analysis suggests a vertical propagation in the middle latitudes of the NH, even though we chose the latitude 50^oN as our representative instead of the latitude 40^oN as García-Herrera et al. [2006] did. Still, this is in good agreement with results from Manzini et al. [2006]; Sassi et al. [2004]. In the coming section the Rossby wave propagation will be further visualized in terms of the EP-flux cross sections.

4.2.3 Zonal flow interaction on the vertical wave propagation

The propagation and dissipation of Rossby waves at middle latitudes and their integration with the zonal mean flow is a widely accepted mechanism behind the ENSO signal in the boreal winter stratosphere (Calvo et al. [2008]; García-Herrera et al. [2006]; Li and Lau [2012]). Our approach to analyse this mechanism has been to study the wave propagation and dissipation in the stratosphere and mesosphere from the result of the CESM1(WACCM) and how they affect the stratospheric branch, as well as the mesospheric branch of the meridional circulation. The deviation from the average state of the meridional circulation are known to cause the deviations in the zonal mean zonal wind and temperature in the boreal winter and will be explained in this section. For comparability reasons with García-Herrera et al. [2006], parameters such as the EP-flux and the EP-flux divergence have been cropped to the same vertical range (i.e. 50 - 0.1 *hPa* or 20 - 60 *km*).

The wave propagation can be studied by looking into the EP-flux. The EP-flux vectors are considered as a measure of the wave propagation from one latitude to another (García-Herrera et al. [2006] and references therein). The composite differences (El Niño minus La Niña) of the EP-flux anomalies are displayed in Figure 4.10. Overall, a very discernible strengthened upward propagation in the NH and a reduced propagation in the SH at middle latitudes is observed. Again, the explanation is the cycle of the zonal mean zonal winds (Figure 4.1b): westerly winds in the NH and easterly winds in the SH are seen during the boreal winter. A clear poleward/upward channel around 60^oN (even towards higher latitudes in Figure 4.10b) reaches the heights at around 0.5 *hPa*, where they bends towards the equator at lower heights ($\sim$ 1*hPa*). This westward tilt is a good indicator of an efficient vertical propagation. Furthermore, this result is consistent with the pattern seen in Figure 4.6. The Rossby wave propagation is reflected by this evidence of intense upward propagation in the NH in Figure 4.10.

The anomalies of the EP-flux divergence are shown in Figure 4.11a. By taking the divergence of the EP-flux, the forcing on the mean flow by the wave perturbation can be measured directly (Calvo et al. [2008] and references therein). Negative values of the EP-flux divergence indicate regions of Rossby wave dissipation (convergence zones) and transmission of momentum on to the zonal mean flow (Figure 4.12). The EP-flux divergence reveals a more convergent pattern in a large part of the middle and upper stratosphere at winter mid- and high latitudes. This convergence refer to the deceleration of the westerlies and could explain the appearance of Figure 4.12, where the westerlies in the stratosphere at middle latitudes has decreased substantially. The divergence regions in Figure 4.11a could indicate the acceleration of the westerlies in Figure 4.12.

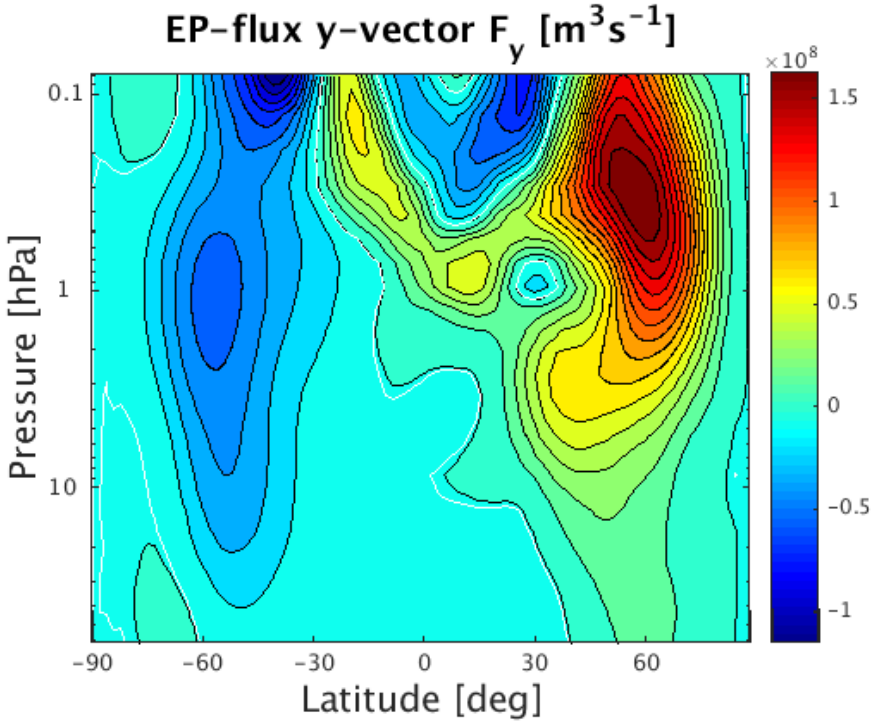

(a)

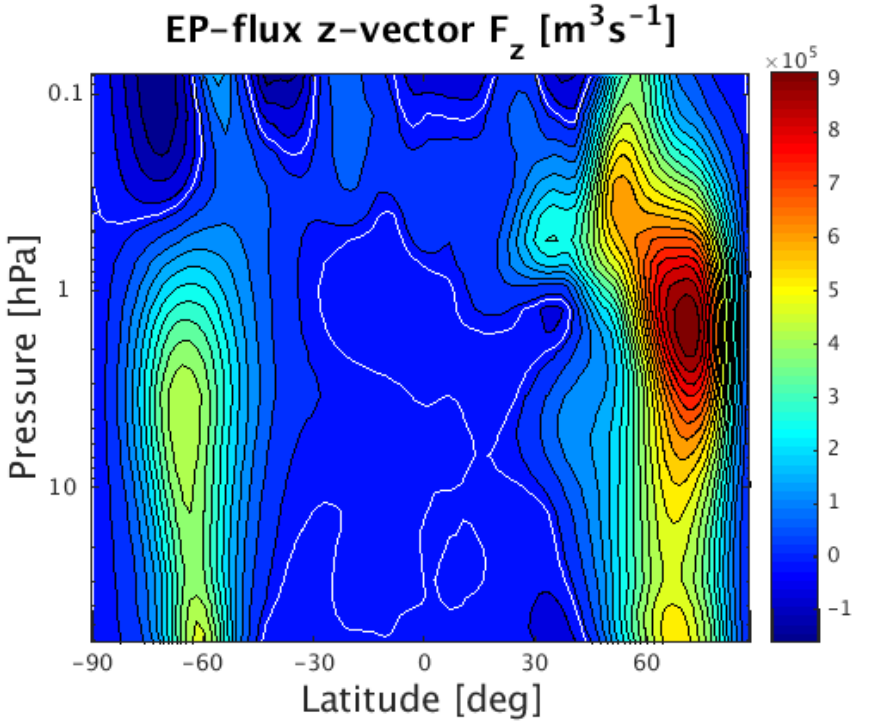

(b)

Figure 4.10: Composite differences (El Niño minus La Niña) for the EP-flux anomalies after an El Ninño event. The vectors have been scaled by the inverse density to make them more apparent in the stratosphere. For the EP-flux y-vector $\mathcal{F}_\mathbf{y}$: positive (negative) values indicate northward (southward) motion, whereas for the EP-flux z-vector $\mathcal{F}_\mathbf{z}$: positive (negative) values indicate upward (downward) motion. Thin white line marks the boundary line between positive and negative values. Units are $m^3 s^{-1}$.

The effect of the ENSO signal in the stratosphere is today well understood. However, the impact the ENSO effect has on the mesosphere has been less studied. As mentioned in Section 2.3.6, there are other circulations of interest outside the stratosphere. In the mesosphere, the mean meridional circulation are driven by small-scale gravity waves. Therefore, the composite differences (El Niño minus La Niña) for the gravity wave drag anomalies have been included (Figure 4.11b). Above the lower stratosphere and beyond the lower mesosphere between the extratropical regions to the polar regions, an anomalous eastward gravity wave drag is visible for the NH winter. In contrast, an anomalous eastward gravity drag is also visible in the SH summer and might explain the increased westerlies from the lower mesosphere tilting towards the mesopause from the middle- to high latitudes.

Increased wave propagation into the stratosphere at middle- and high latitudes lead to the EP-flux convergence observed between 50 - 0.1hPa in Figure 4.10. The convergence of the EP-flux is a possible explanation for the weakening of the westerlies (Figure 4.12) in the lower stratosphere at middle- and high latitudes. At the same latitudes but from the middle stratosphere to the middle mesosphere, a strengthening of the westerlies can be seen and the anomalous eastward gravity wave drag (Figure 4.11b) could explain it and furthermore modify the residual circulation in the mesosphere (e.g Li et al. [2013]).

Until now, we have studied the ENSO signal due to upward vertical propagation. The cause for this is the vertical propagation and dissipation by Rossby waves during warm ENSO events as discussed earlier. For these events, we saw in Figure 4.10 how the convergence zones of the EP-flux increases at higher levels and thereby modulates the BDC. During extreme events, not only the zonal temperatures and the wave driving is modified but the meridional circulation is also affected. Observations from studies such as Calvo et al. [2010, 2008]; García-Herrera et al. [2006]; Manzini [2009] point out that during a warm ENSO event, the stratospheric branch of the mean meridional circulation is strengthened during the boreal winter (Figure 4.13).

For the NH in Figure 4.12, the eastward anomaly is consistent with the Coriolis force acting on the enhanced pole-to-pole transport in the mesosphere. Below, in the stratosphere, the westward anomaly is consistent with the weakened BDC. In the SH, an opposite anomaly can be observed in the mesosphere (caused here again by the Coriolis force), as well as a weakened BDC. However, when interpreting the zonal mean zonal wind composite, one needs to take into account not only the divergence of the EP-flux and the gravity wave drag but also the meridional circulation (see Equation 2.4). The time limitation of this project was another factor that restricted us to make further analysis into this like the authors of Li et al. [2013] did.

Li et al. [2013] focused on studying the influence of the ENSO in the mesosphere as the understanding of this layer is not as clear as the ENSO signal in the stratosphere. In their study, a former WACCM version (WACCM3.5) was used but with the same parametrized gravity wave (GW) drag (used in their model version and ours, details can be found in Li et al. [2013]; Marsh et al. [2013] and references therein). They show cross sections of the WACCM3.5 responses to ENSO in the EP-flux divergence of the (resolved) Rossby waves in the model, the parametrized gravity wave drag and the total effects of these effects combined. These effects are clearly getting enhanced by the warm ENSO influence, corresponding to decelerated zonal mean zonal wind. These findings are consistent with the WACCM1b results from García-Herrera et al. [2006]. For the NH mesosphere however, WACCM3.5 shows an anomalous eastward wave forcing in the total wave forcing. This results is confirmed by an anomalous eastward gravity wave drag.

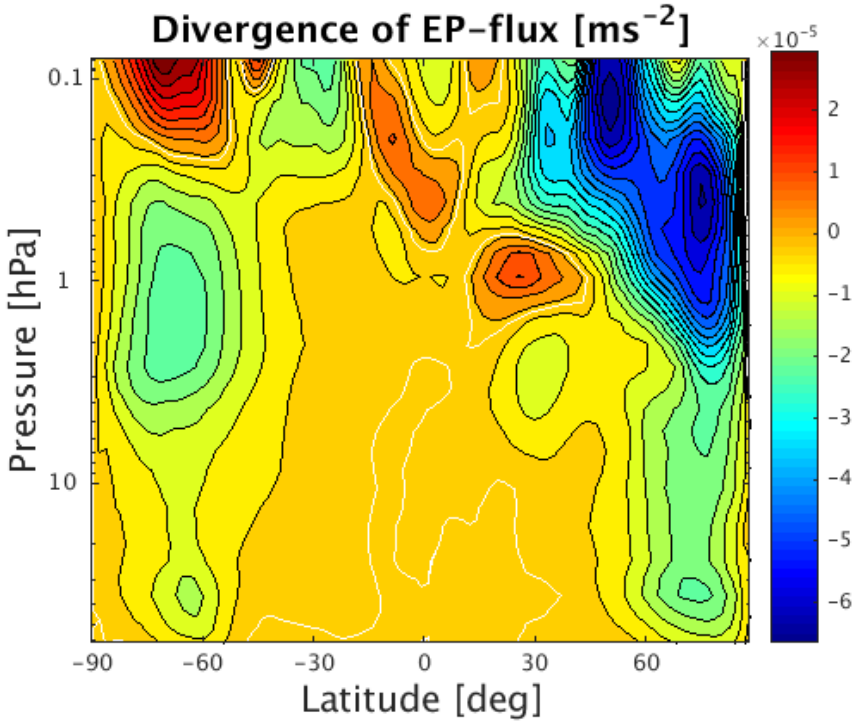

(a)

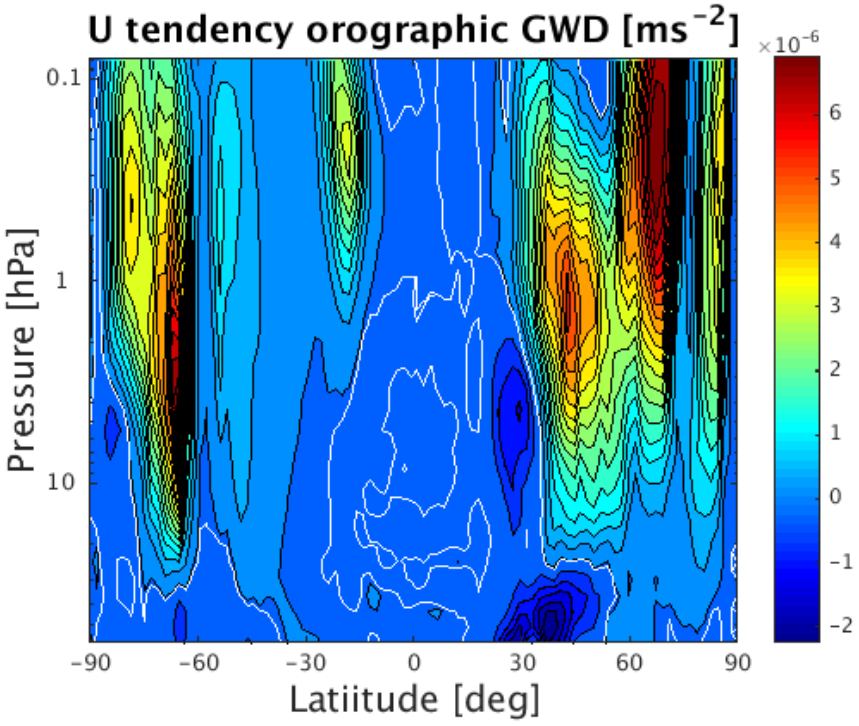

(b)

Figure 4.11: Composite differences (El Niño minus La Niña) for the a) EP-flux divergence anomalies (ms^{-2}) and b) orographic gravity wave anomalies drag with respect to U tendencies (ms^{-2}) after an El Niño event. Thin white line marks the boundary line between positive and negative values.

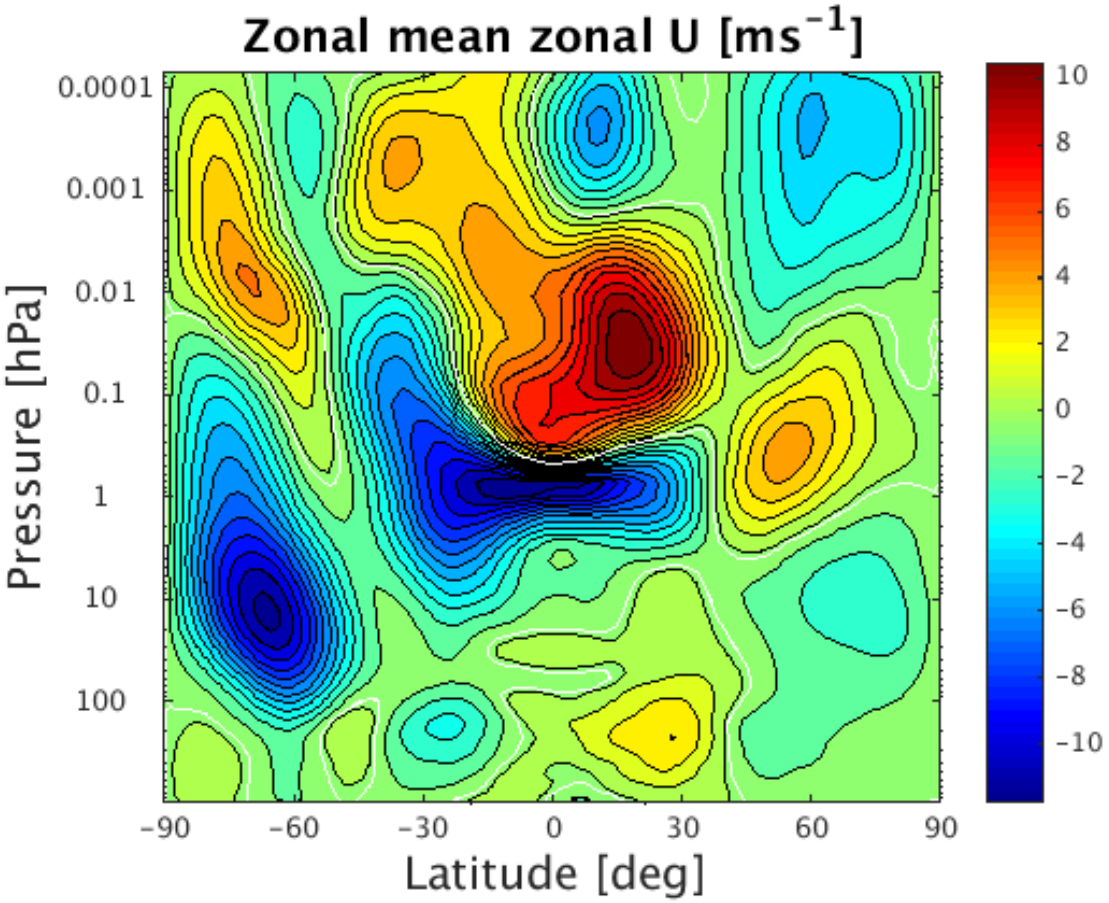

Figure 4.12: Composite differences (El Niño minus La Niña) for the zonal mean wind U (ms^{-1}) anomalies after an El Niño event. Thin white line marks the boundary line between positive and negative values.

4.2.4 Impact on the mean meridional circulation

Previous studies revealed that warm ENSO events intensify the Rossby wave propagation and dissipation at middle and high latitudes in the NH (Calvo et al. [2010]; García-Herrera et al. [2006]; Li and Lau [2012]). Furthermore, they decelerate the stratospheric polar vortex and enhance the stratospheric branch of the BDC (Butchart et al. [2010, 2006]; Calvo et al. [2010]). This residual circulation is an good approximation of the movement of air parcels in the middle atmosphere. It is an eminent fact that this circulation is driven by planetary waves and shapes the thermal structure of the stratosphere (Andrews et al. [1987]). In Figure 4.13 the two components of the residual circulation response during warm ENSO events have been depicted.

For the meridional TEM velocity anomalies, $\overline{V}^*$ (Figure 4.13a), significant values can be observed in the tropical troposphere region. In the same region, significant positive values can be seen in the lower mesosphere/upper stratosphere followed by significant negative values overhead. For most of the latitudes, from the upper troposphere/lower stratosphere to the stratopause, values are low. From the middle mesosphere up to the mesopause/lower thermosphere, a strongly enhanced northward mesospheric branch can clearly be observed stretching from the south pole over to the north pole. From the upper troposphere at NH polar latitudes a northward motion stretches up to the core in the middle mesosphere where the motion is the

strongest.

In Figure 4.13b the vertical TEM velocity anomalies, $\overline{W}^*$, have been depicted. From the upper troposphere at polar latitudes a branch tilting upward to the extratropical lower mesosphere is visible. Then this tilting branch moves toward an oncoming northward branch of $\overline{V}^*$ in the tropical region in the lower mesosphere/upper stratosphere mentioned for Figure 4.13a. Otherwise, an enhanced downward branch through the NH polar mesosphere can be seen, sinking down into the lower mesosphere/upper stratosphere. In the SH summer significant values can observed near the upper troposphere, indicating enhanced upward motion there. From here up to the lower mesosphere it is hard to describe the situation but with very weak positive values it could be an indication of a weak ascent. Through the middle mesosphere significant positive values are observed indicating enhanced upward motion. Overall the pattern from pole-to-pole above the tropopause and below the stratopause is hard to grasp.

As planetary waves propagate vertically into the stratosphere, they are refracted towards the equator (Figure 4.10), deposit easterly momentum and decelerate the flow (Figure 4.11a)(García-Herrera et al. [2006] and references therein). To compensate for the deceleration (indicated by the negative values in the EP flux divergence anomalies (Figure 4.11a), the residual circulation moves poleward (Figure 4.13) and thereby causes adiabatic cooling in the tropics and warming in the extratropics. Thus enhancement of the residual circulation in Figure 4.13 could explain the observed warming in the polar region in Figure 4.9. This relationship was introduced by (Newman et al. [2001]), whom used reanalysis data (NCEP-NCAR)[I] to show that an enhanced negative EP-flux divergence decelerates the zonal mean flow and warms the polar stratosphere.

The intensification of the residual circulation is likely a result of the anomalous wave dissipation indicated by the negative values in the EP-flux divergence anomalies (Figure 4.11a). This enhancement of the divergences indicates an increase of the wave mean flow interaction and an eventual weakening of the zonal flow. However, as stated before, the picture is less clear below the stratopause in the mean meridional circulation pattern. The results shown up to now are consistent in terms of the residual circulation, EP-flux vectors and temperature. The overall circulation picture would be an ascending motion at SH polar latitudes, continuing as a poleward branch in the mesosphere with descending motion at the NH polar latitudes towards the upper stratosphere. This descent meets an opposing upwards tilting branch from the tropopause at polar latitudes in the NH winter, leading to a weakening of the BDC.

[I]The NCEP/NCAR (National Center for Environmental Prediction/National Center for Atmospheric Research) reanalysis is a global gridded data set from 1948 to the present. The data set represents the state of the Earth's atmosphere, incorporation of observations and numerical weather prediction model output from 1948 til present. https://en.wikipedia.org/wiki/NCEP/NCAR_Reanalysis

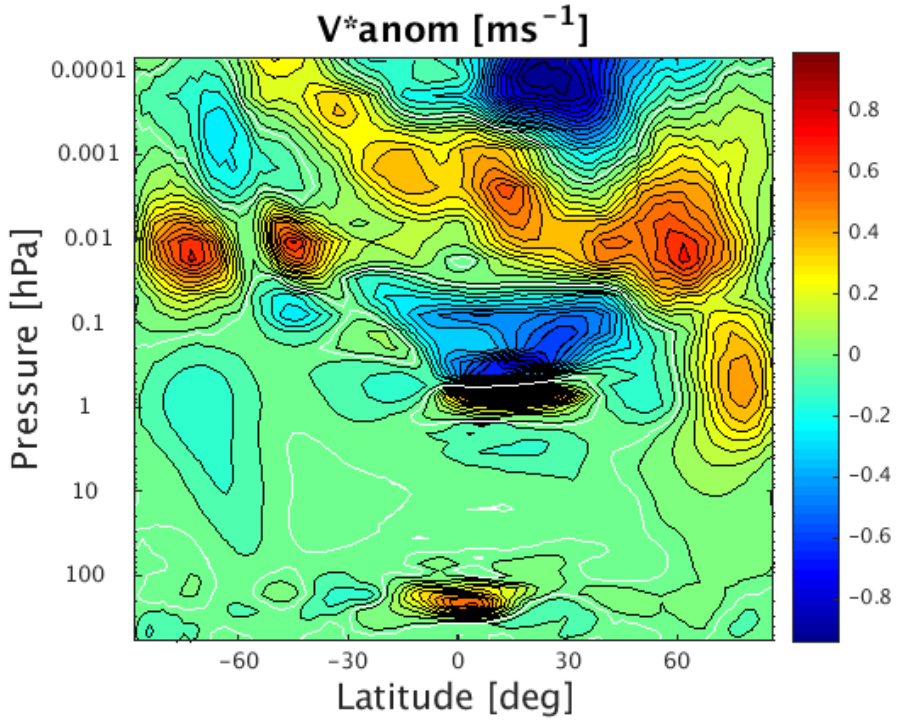

(a)

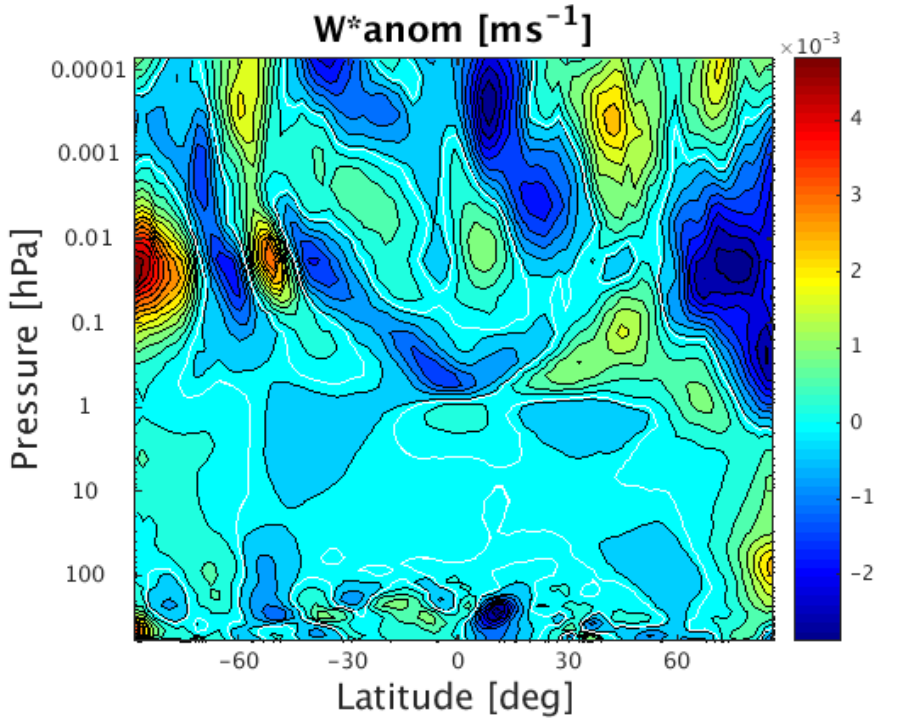

(b)

Figure 4.13: Composite differences (El Niño minus La Niña) for the mean meridional TEM velocities anomalies after an El Niño event. For the meridional TEM velocity $\overline{V}^*$ anomalies: positive (negative) values indicate northward (southward) motion, whereas for the vertical TEM velocity $\overline{W}^*$ anomalies: positive (negative) values indicate upward (downward) motion. Thin white line denotes boundary line between positive and negative values. Units are ms^{-1}.

4.3 Tracer transport

Transport refers to processes where air motion carry physical properties or chemical compounds from one region to another. Through transport, different chemical compounds with different sources start to interact (Brasseur et al. [1999, chapter 2], Wallace and Hobbs [2006, chapter 5]). A great part of the chemistry of the stratosphere involves ozone, which is very active and driven by intense solar radiation and continuous influx of compounds from the troposphere. This concentration of ozone has a strong impact on the diabatic heating, which in turn influences both the temperature and wind. As a consequence the winds influence the ozone distribution through transport while the temperatures affect the chemical reaction rates related to ozone.

Rising motion in the tropics brings source gases away from the troposphere. These source gases are then transported poleward in the lower stratosphere. However, transport is more prominent in the winter hemisphere than in the summer hemisphere. Not only does the Rossby waves drive the mean circulation but they are also behind the quasi-horizontal mixing of chemical components. Air motions caused by Rossby waves tend to occur along potential temperature surfaces, and are thus approximately adiabatic Shepherd [2007]. The breaking of Rossby waves leads to mixing of chemical components and is an efficient transport mechanism in the stratospheric surf zone (Brasseur et al. [1999]; Shepherd [2007]). In this section the behaviour of chemical components such as the N_2O, $CH4$ and O_3 during a warm ENSO event will be investigated.

4.3.1 The ENSO signal in the chemical compounds

Studying the transport in the middle atmosphere provides insight of its key features such as the stratospheric surf zone and mixing barriers (Brasseur et al. [1999]; Shepherd [2007]). The winter stratosphere is characterized by very low temperatures due to the absence of solar heating and a strong eastward flow around the pole (the "polar vortex"), as illustrated in Figure 2.6. This condition permits propagation of the planetary waves into the winter stratosphere as described in Section 2.2.1.

From the climatology distribution of CH_4 (Figure 4.5b), we remember that abundance of CH_4 is found in the troposphere due to upwelling and decreased concentration in the upper stratosphere due to photochemical dissociation. In order to understand the behaviour of the different tracers, we need to study them together with the closely linked residual circulation. From the previous section, the results show a strong effect in the mesosphere with a strengthened pole-to-pole circulation. In the NH polar stratosphere there is weak ascent and a pattern of BDC weakening.

In light of the values found for the lower middle atmosphere in Figure 4.14a, increased values of CH_4 are found from equator to NH pole in the lower mesosphere/upper stratosphere. This could be explained by the upward tilting branch from the upper troposphere at the NH polar latitudes. The negative values observed at the polar NH stratosphere could be explained by the downwelling discussed earlier. Knowing the fact that CH_4 and N_2O are similar in appearance (verified in Figure 4.14a and 4.14b), similar argumentation will be used when discussing Figure 4.14b. For $N2O$ in Figure 4.14b we again see increased but weaker values from equator to NH pole, again explained by the weakened BDC in this region.

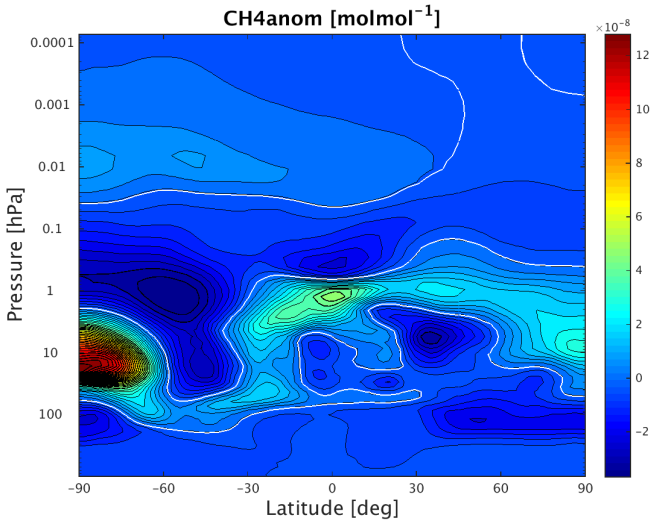

(a)

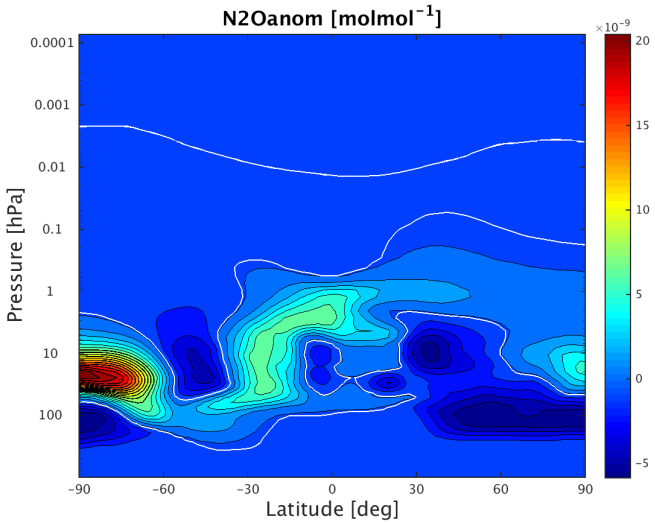

(b)

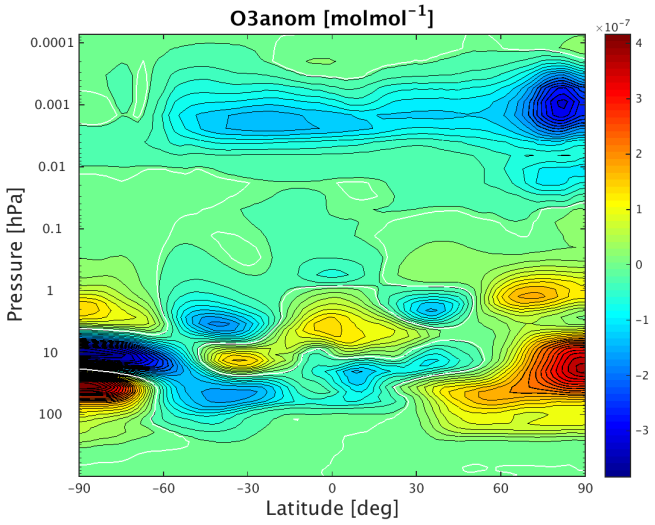

(c)

Figure 4.14: Composite differences (El Niño minus La Niña) for the zonal mean CH_4 anomalies (top), N_2O anomalies (middle) and O_3 anomalies (bottom). Thin white line denotes boundary line between positive and negative values. Units are $molmol^{-1}$.

Previous modelling studies such as Cagnazzo et al. [2009]; Randel et al. [2009] showed reduced ozone concentration over the tropics and accumulation of ozone at high latitudes in the NH, indicating stronger diabatic downwelling during warm ENSO in this region. These results suggested a strengthening of the BDC, induced by the vertical propagation of waves (shown in Figure 4.10). In the study by Randel et al. [2009], a different methodology has been used by the authors. They plotted meridional cross sections of zonal mean ozone regressed onto the Multivariate ENSO index (MEI). They observe a strong ENSO signal for both the temperature and ozone concentration in the tropical lower stratosphere in both the WACCM model (a previous version) and observational data set. Their results prove a strong relationship in the spatial patterns of ENSO signals between the model and observations for both temperature and ozone concentration. However, our results (Figure 4.9 and 4.14c) do not show such striking behaviours or consistency at all.

As suggested by the chemistry-climate models (Butchart et al. [2010, 2006]), the BDC is strengthening and will continue to do so throughout the twenty-first century. Enhanced BDC means greater mass transport from the tropics to the extratropics. This suggests that the tropical ozone concentration may never recover to pre-industrial levels, while on the other hand the extratropical ozone concentration will become larger than ever before (Shepherd [2008]; Waugh et al. [2009]). Changes in the horizontal gradient of ozone concentration can have major dynamical feedbacks in the stratosphere and troposphere. For instance, changes in the BDC could be linked to changes in tropical activity in the North Atlantic (Gerber et al. [2012] and references therein). On the other hand, analysis by Engel et al. [2009] of stratospheric tracers over the last decades suggest a weakening of mass transport. From their stratospheric observations of long-lived tracers variability, they suggest it is caused by inter-annual variations in transport. These inter-annual variations could explain the observed weakening of the BDC in our results.

In Figure 4.14c the impact of the ENSO on ozone concentration is shown. In the NH polar mesosphere, decreased ozone concentration fits well with the anomalous downwelling in the secondary ozone layer. This reduction of ozone is consistent with warmer temperature observed in Figure 4.9 (Tweedy et al. [2013]). This is because ozone and temperature are anti-correlated, at least during night-time (Tweedy et al. [2013]). The warm anomaly in Figure 4.9 clearly indicates low ozone concentration anomalies in the secondary and tertiary ozone layers. In the SH, there is a strong warm anomaly in upper troposphere/lower stratosphere. A similar anomaly can be found for N_2O and CH_4 but in the lower stratosphere instead. Even though the main priority of this thesis is to study the boreal winter, we will discuss the austral summer briefly. For all the chemistry figures with respect to the ENSO (i.e Figure 4.14), strong positive/negative anomalies in the stratosphere can be detected for all our chosen chemistry compounds.

For the $\overline{W}^*$, an observed weak ascent at high latitudes turns into a weak descent at middle latitudes in the SH summer. This statement is also supported by the weak $\overline{V}^*$ indicating southward motion, helping to form this looping cell. Then this cell could explain the strong anomalies we observe, at least for methane and nitrous oxide (Figure 4.14a and 4.14b respectively). If we were to use the same argumentations for explaining the observed ozone anomaly (SH high latitudes), then upward motion would bring colder air from below containing air with low ozone concentration. Furthermore, the residual circulation would advect temperature into the area and make it colder as we observe in Figure 4.9. This movement could explain the deficit of ozone in the middle stratosphere at SH polar latitudes. However, it does not end here as a strong positive anomaly is observed below in the lower stratosphere. The residual circula-

tion can not explain this behaviour and makes us wonder if this could be remains from the SH spring.

We quickly realized that this is can not be explained straightforwardly. The closely linked residual circulation has been studied; for CH_4 and N_2O there is a qualitative agreement, while the impact of the residual circulation on O_3 is less clear. More investigation will be needed. For instance, how will the chemistry look like if we consider lags from the previous season, e.g. spring in the SH. Their significance also needs to be looked into. In order to do so, a full chemistry budget analysis would be needed. Unfortunately due to time limitations we did not focus on this. Further work could perhaps answer these questions more thoroughly.

CHAPTER 5

Future Work

The results presented in this project has demonstrated the upward wave propagation into middle atmosphere and its impact, however it could be further developed in a number of ways:

Further analysis of the available model experiment

A strong signature in the mesosphere was demonstrated being consistent in terms of the wave fluxes, meridional circulation as well as temperature and winds, and impact on transport and chemistry of key trace species. The results are not consistent with previous investigations, and methodological differences should be further explored.

Investigate the hemispheric differences and their seasonal variabilities with respct to ENSO

By expanding the study to focus on both hemispheres, we can look more into the hemispheric differences as well as their seasonal variabilities. Then we could see the differences between the SH winter versus the NH winter and similarily for other seasons. Seasonal lags would be interesting to study in terms of understanding the transport and chemistry of ozone in particular. Perhaps comparisons with other chemistry models as well could be done and see what kind of differences/similiarities come out.

Expand the WACCM model with more ensemble runs

Comparisons of several data runs could give provide more information to understand their response to extreme cases of ENSO and their significance. Exploring their statistics such as their significance, correlation would also provide a broader spectre of understanding.

CHAPTER 6

Conclusion and Summary

The El Niño-Southern Oscillation (ENSO) has its origins in the tropical Pacific ocean, yet it has a great impact on the Northern Hemisphere (NH) wintertime variability. The ENSO affects the circulation in the middle atmosphere through the propagation of the planetary Rossby waves and gravity waves. To explore this phenomenon, data sets were made available to me. They were computed by the latest version of the Whole Atmospheric Community Climate Model (WACCM), the CESM1(WACCM). This model is a part of the phase 5 of the Coupled Model Intercomparison Project (CMIP5). The observed Hadley Center Sea Ice and Sea Surface Temperature (HadISST) data set was used in the CESM1(WACCM) model and gave us one output referred to as the control-run (CTRL-run). Then a filter was applied to the same HadISST data set to give us a second output that only included the ENSO-related component. This data set is referred to as the ENSO-related-run (ENSO-run) and our study is based on this simulation.

Our aim was to study the climatology of the temperature, the zonal mean wind, the wave flux vectors and its divergence and the residual circulation. Then we wanted to see how a warm ENSO event affected these parameters. We also looked into how these changes affected the trace gases transport. From our results we observed significant wave-like anomalies in the stratosphere as well as in the mesosphere at middle latitudes with the most efficient wave propagation around 50^oN. We have shown that the wave activity is reflected in the pattern of the EP-flux. Results show that this wave propagation is strongly influenced by the zonal mean winds. This relationship is explained by the Charney-Drazin criteria: during the boreal winter, if stratospheric winds are westerly and their velocity is less than a critical value (which is strongly dependent the wave number and the latitude), then vertical wave propagation is possible.

The ENSO also generates significant anomalies in the zonal field. The zonal mean temperature anomalies are observed in both the tropical and polar regions of the NH middle atmosphere. The modulation of the residual circulation (ascent in the tropics and descent in the polar region) are the reason for these temperature anomalies. During a warm ENSO event we observe an enhancement of the vertical wave propagation at middle latitudes and a divergence of the wave flux that indicates the weakening of the zonal mean zonal wind due to deposit of easterly momentum. Combined, this modulates our residual circulation. For the NH polar stratosphere a

weak ascent and a pattern of weakened BDC is observed, whereas a strong effect in the mesosphere with a strengthened pole-to-pole circulation is seen. This strengthened mesospheric branch explains the observed anomalous temperatures observed in the mesosphere. The residual circulation is closely linked to the trace gases transport and for methane and nitrous oxide there is a qualitative agreement, while impact of the residual circulation on the ozone is less clear. Within this model run, consistency is observed between the residual circulation, EP-flux vectors and temperature. Originally Figure 6.1 applied to the stratosphere only but the main mechanisms fit pretty well with our observation of the ENSO signal in the mesosphere.

Our study reveals similar findings as previous modeling studies but also a few differences. In certain aspects of our results there seem to be some inconsistency with other studies. In terms of the changes in temperature and tracers due to the ENSO, we observe a strong anomaly in the SH summer that is not observed in previous work. While other studies report strengthened BDC, we observed a weakened BDC circulation. The novelty of our approach enabled us to have a new point of view on the El Niño-Southern Oscillation and the observed data is somehow different than reported in previous studies. Further work could investigate these divergence and possibly extract new theories from their interpretation.

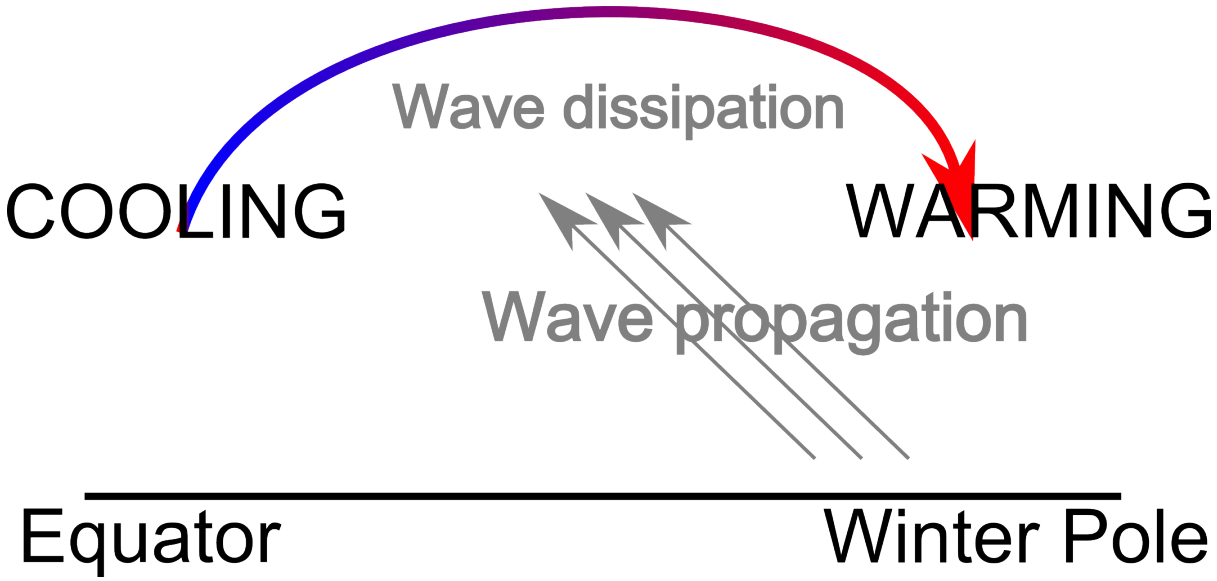

Figure 6.1: Orginal figure by Calvo et al. [2008]: The main mechanisms involved in the propagation of the ENSO signal in the stratosphere. The thin grey arrow indicate the anomalous wave propagation and point to the dissipation region. The thick blue/red arrow indicate the air movement by the intensification of the stratospheric mean meridional circulation from anomalous dissipation. As a result the air cools down in the tropical stratosphere and warms up at polar latitudes in the Northern Hemisphere as is indicated in the figure

.

Appendix

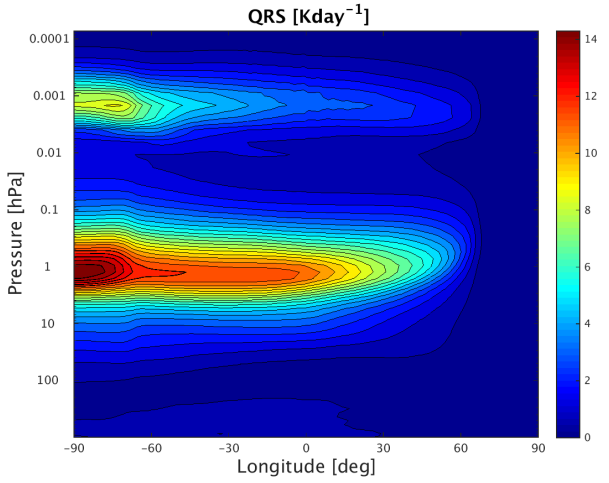

(a)

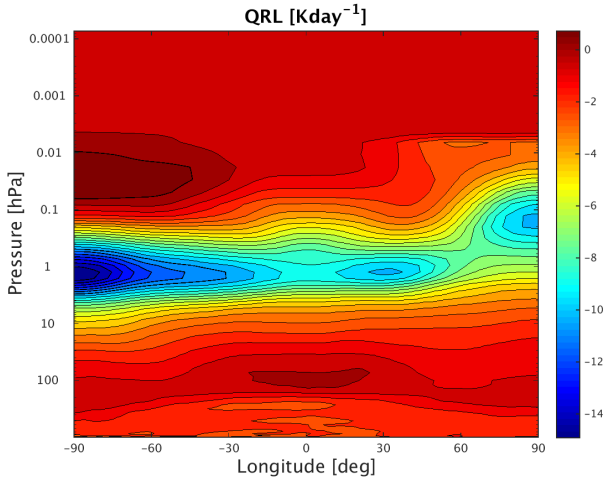

(b)

Figure 6.2: Winter climatology (December-January-February) of a) the diabatic heating and b) radiative cooling as function of latitude and pressure for the period 1955-2001. Units are $Kday^{-1}$.

Bibliography

Andrews, D., Holton, J., and Leovy, C. (1987). *Middle atmosphere dynamics*. Academic press.

Andrews, D. and McIntyre, M. (1976). Planetary waves in horizontal and vertical shear: The generalized eliassen-palm relation and the mean zonal acceleration. *Journal of the Atmospheric Sciences*, 33(11):2031–2048.

Andrews, D. and McIntyre, M. (1978). An exact theory of nonlinear waves on a lagrangian-mean flow. *Journal of Fluid Mechanics*, 89(04):609–646.

Baldwin, M., Gray, L., Dunkerton, T., Hamilton, K., Haynes, P., Randel, W., Holton, J., Alexander, M., Hirota, I., Horinouchi, T., Jones, D., Kinnersley, J., Marquardt, C., Sato, K., and Takahasi, M. (2001). The quasi-biennial oscillation. *Reviews of Geophysics*, 39(2):179–229.

Bjornsson, H. and Venegas, S. (1997). A manual for EOF and SVD analyses of climatic data. *CCGCR Report*, 97(1).

Brasseur, G., Orlando, J., Tyndall, G., et al. (1999). *Atmospheric chemistry and global change*. Oxford University Press.

Butchart, N., Cionni, I., Eyring, V., Shepherd, T., Waugh, D., Akiyoshi, H., Austin, J., Brühl, C., Chipperfield, M., Cordero, E., et al. (2010). Chemistry-climate model simulations of twenty-first century stratospheric climate and circulation changes. *Journal of Climate*, 23(20):5349–5374.

Butchart, N., Scaife, A., Bourqui, M., De Grandpré, J., Hare, S., Kettleborough, J., Langematz, U., Manzini, E., Sassi, F., Shibata, K., et al. (2006). Simulations of anthropogenic change in the strength of the brewer–dobson circulation. *Climate Dynamics*, 27(7-8):727–741.

Butler, A., Polvani, L., and Deser, C. (2014). Separating the stratospheric and tropospheric pathways of el nino-southern oscillation teleconnections. *Environmental Research Letters*, 9:9.

Cagnazzo, C., Manzini, E., Calvo, N., Douglass, A., Akiyoshi, H., Bekki, S., Chipperfield, M., Dameris, M., Deushi, M., Fischer, A., et al. (2009). Northern winter stratospheric temperature and ozone responses to enso inferred from an ensemble of chemistry climate models. *Atmospheric Chemistry and Physics*, 9(22):8935–8948.

Calvo, N., Garcia, R., Randel, W., and Marsh, D. (2010). Dynamical mechanism for the increase in tropical upwelling in the lowermost tropical stratosphere during warm ENSO events. *Journal of the Atmospheric Sciences*, 67(7):2331–2340.

Calvo, N., García-Herrera, R., and Garcia, R. (2008). The ENSO signal in the stratosphere. *Trends and Directions in Climate Research: Annals of the New York Academy of Sciences*, 1146:16–31.

Charney, J. and Drazin, P. (1961). Propagation of planetary-scale disturbances from the lower into the upper atmosphere. *Journal of Geophysical Research*, 66(1):83–109.

Compo, G. and Sardeshmukh, P. (2010). Removing ENSO-related variations from the climate record. *Journal of Climate*, 23(8):1957–1978.

Cordero, E., Newman, P., Weaver, C., and Fleming, E. (2013). Chapter 6: stratospheric dynamics and the transport of ozone and other trace gases. *Stratospheric Ozone: An Electronic Textbook*.

Engel, A., Möbius, T., Bönisch, H., Schmidt, U., Heinz, R., Levin, I., Atlas, E., Aoki, S., Nakazawa, T., Sugawara, S., et al. (2009). Age of stratospheric air unchanged within uncertainties over the past 30 years. *nature geoscience*, 2(1):28–31.

Fernández, N., Herrera, R., Puyol, D., MartÍn, E., GarcÍa, R., Presa, L., and RodrÍguez, P. (2004). Analysis of the ENSO signal in tropospheric and stratospheric temperatures observed by MSU, 1979-2000. *Journal of climate*, 17(20):3934–3946.

Free, M. and Seidel, D. (2009). Observed el nino-southern oscillation temperature signal in the stratosphere. *Journal of Geophysical Research: Atmospheres (1984–2012)*, 114(D23):11.

Fritts, D. and Alexander, M. (2003). Gravity wave dynamics and effects in the middle atmosphere. *Reviews of Geophysics*, 41(1).

García-Herrera, R., Calvo, Nand Garcia, R., and Giorgetta, M. (2006). Propagation of ENSO temperature signals into the middle atmosphere: A comparison of two general circulation models and ERA-40 reanalysis data. *Journal of Geophysical Research: Atmospheres (1984–2012)*, 111(D06010):14.

Gerber, E., Butler, A., Calvo, N., Charlton-Perez, A., Giorgetta, M., Manzini, E., Perlwitz, J., Polvani, L., Sassi, F., Scaife, A., et al. (2012). Assessing and understanding the impact of stratospheric dynamics and variability on the earth system. *Bulletin of the American Meteorological Society*, 93(6):845–859.

Hardiman, S., Butchart, N., Haynes, P., and Hare, S. (2007). A note on forced versus internal variability of the stratosphere. *Geophysical research letters*, 34(12).

Hartmann, D. (1994). *Global physical climatology*, volume 56. Academic press.

Holton, J. and Hakim, G. (2012). *An introduction to dynamic meteorology*, volume 88. Academic press.

Li, T., Calvo, N., Yue, J., Dou, X., Russell, J., Mlynczak, M., She, C., and Xue, X. (2013). Influence of el niño-southern oscillation in the mesosphere. *Geophysical Research Letters*, 40(12):3292–3296.

Li, Y. and Lau, N. (2012). Impact of ENSO on the atmospheric variability over the north atlantic in late winter-role of transient eddies. *Journal of Climate*, 25(1):320–342.

Manzini, E. (2009). ENSO and the stratosphere. *Atmospheric Science*, 2:749–750.

Manzini, E., Giorgetta, M., Esch, M., Kornblueh, L., and Roeckner, E. (2006). The influence of sea surface temperatures on the northern winter stratosphere: Ensemble simulations with the MAECHAM5 model. *Journal of climate*, 19(16):3863–3881.

Marsh, D., Mills, M., Kinnison, D., Lamarque, J., Calvo, N., and Polvani, L. (2013). Climate change from 1850 to 2005 simulated in CESM1(WACCM). *Journal of Climate*, 26(19):7372–7391.

Newman, P., Nash, E., and Rosenfield, J. (2001). What controls the temperature of the arctic stratosphere during the spring? *Journal of geophysical research*, 106(D17):19999–20010.

Newman, P. and Todara, R. (1996). Stratospheric ozone: An electronic textbook. *NASA GSFC: Available at/http://www. ccpo. odu. edu/SEES/ozone/oz_class. ht mS (20100610)*.

Penland, C. and Magorian, T. (1993). Prediction of nino 3 sea surface temperatures using linear inverse modeling. *Journal of Climate*, 6(6):1067–1076.

Penland, C. and Matrosova, L. (2006). Studies of el niño and interdecadal variability in tropical sea surface temperatures using a nonnormal filter. *Journal of climate*, 19(22):5796–5815.

Penland, C. and Sardeshmukh, P. (1995). The optimal growth of tropical sea surface temperature anomalies. *Journal of climate*, 8(8):1999–2024.

Plumb, R. (2002). Stratospheric transport. *Journal of the Meteorological Society of Japan. Ser. II*, 80(4B):793–809.

Randel, W., Garcia, R., Calvo, N., and Marsh, D. (2009). ENSO influence on zonal mean temperature and ozone in the tropical lower stratosphere. *Geophysical Research Letters*, 36(15):5.

Rayner, N., Parker, D., Horton, E., Folland, C., Alexander, L., Rowell, D., Kent, E., and Kaplan, A. (2003). Global analyses of sea surface temperature, sea ice, and night marine air temperature since the late nineteenth century. *Journal of Geophysical Research: Atmospheres (1984–2012)*, 108(D14).

Sandeep, S., Stordal, F., Sardeshmukh, P., and Compo, G. (2014). Pacific walker circulation variability in coupled and uncoupled climate models. *Climate Dynamics*, 43(1-2):103–117.

Sassi, F., Kinnison, D., Boville, B., Garcia, R., and Roble, R. (2004). Effect of el niño–southern oscillation on the dynamical, thermal, and chemical structure of the middle atmosphere. *Journal of Geophysical Research: Atmospheres (1984–2012)*, 109(D17).

Shepherd, T. (2007). Transport in the middle atmosphere. *Journal of the Meteorological Society of Japan. Ser. II*, 85:165–191.

Shepherd, T. (2008). Dynamics, stratospheric ozone, and climate change. *Atmosphere-Ocean*, 46(1):117–138.

Solomon, A. and Newman, M. (2012). Reconciling disparate twentieth-century indo-pacific ocean temperature trends in the instrumental record. *Nature Climate Change*, 2(9):691–699.

Thompson, R., Dlugokencky, E., Chevallier, F., Ciais, P., Dutton, G., Elkins, J., Langenfelds, R., Prinn, R. G., Weiss, R., Tohjima, Y., et al. (2013). Interannual variability in tropospheric nitrous oxide. *Geophysical Research Letters*, 40(16):4426–4431.

Tweedy, O., Limpasuvan, V., Orsolini, Y., Smith, A., Garcia, R., Kinnison, D., Randall, C., Kvissel, O., Stordal, F., Harvey, V., et al. (2013). Nighttime secondary ozone layer during major stratospheric sudden warmings in specified-dynamics WACCM. *Journal of Geophysical Research: Atmospheres*, 118(15):8346–8358.

Wallace, J. and Hobbs, P. (2006). *Atmospheric science: an introductory survey*, volume 92. Academic press.

Waugh, D., Oman, L., Kawa, S., Stolarski, R., Pawson, S., Douglass, A., Newman, P., and Nielsen, J. (2009). Impacts of climate change on stratospheric ozone recovery. *Geophysical Research Letters*, 36(3).

Wolter, K. and Timlin, M. (2011). El niño/southern oscillation behaviour since 1871 as diagnosed in an extended multivariate ENSO index (MET.ext. *International Journal of Climatology*, 31(7):1074–1087.

Yulaeva, E. and Wallace, J. (1994). The signature of ENSO in global temperature and precipitation fields derived from the microwave sounding unit. *Journal of climate*, 7(11):1719–1736.